A Nanosecond Surface Dielectric Barrier Discharge Operating Under Altitude Conditions for Aeronautics Applications

Nicolas Bénard, Kossi Djidula Bayoda, Arthur Claude Aba'a Ndong, Éric Moreau

A Nanosecond Surface Dielectric Barrier Discharge Operating Under Altitude Conditions for Aeronautics Applications

Nicolas Benard, Kossi Djidula Bayoda, Arthur Claude Aba'a Ndong, and Eric Moreau

***Abstract*— The objective of this paper is to investigate the influence of environmental conditions on a nanosecond pulsed dielectric barrier discharge (NP-DBD). A test chamber where pressure and temperature can be changed to match with realistic altitude conditions has been used. Electrical and optical characterizations of the NP-DBD are proposed for pressure and temperature changes in range related to flow control applications. In particular, the influence of low pressure is investigated. The results indicate that a reduction in pressure leads to a more diffuse plasma layer that further extends with a reducing ambient pressure. The energy dissipated by the discharge increases with a reducing pressure. Regardless of the pressure level, the heat released by the NP-DBD leads to the formation of a pressure wave propagating at sound speed. A good correlation was found between the extension of the plasma layer and the planar part of the produced pressure wave. Similar electrical characterization has been conducted when the temperature is reduced, while the pressure is maintained at an atmospheric level. It was shown that temperature has the minor effect on the discharge characteristics, but lower is the temperature and lower is the deposited energy. In the final part, the influence of the altitude effect is studied by combining pressure and temperature changes. It results that the pressure variation dominates the temperature influence. As a result, higher energy deposition is reported when the altitude is increased. The effect of changes in the pressure and temperature is interpreted as an effect of changes in the gas density. It is concluded that the gas density, N, is an important parameter for studying DBD under the altitude conditions. Indeed, quantities such as the plasma extent and the deposited energy scale with $N^{-0.5}$. However, the gas density does not consider changes in the dielectric permittivity, which restricts the use of the gas density matching method to altitudes with moderate ambient temperature.**

***Index Terms*— XXXXX.**

I. Introduction

PLASMA discharges for flow control have emerged as alternative to mechanical systems over the last decade. Recently, interest has arisen in the use of nanosecond pulsed dielectric barrier discharges (NP-DBDs) for the manipulation of turbulent flows. Originally applied to ozone generation and the destruction of pollutants, these discharges also have a high potential for mitigating separated flows at regimes approaching realistic conditions for applications in aerodynamics [1]–[5]. The current knowledge is not clear regarding the precise effect of this type of discharge. Some authors suggest that the control mechanism is related to the production of vortical flow structures or to interactions between natural vortical flow structures and a local pressure change imposed by the discharge. Another possible reason for the effectiveness of NP-DBDs is its capability to impose the turbulent flow regime in the boundary layer developing the downstream discharge. Unlike typical ac DBDs for which the electric wind is fully responsible for the control mechanism, the NP-DBDs do not produce electric wind [6]. Instead, the rapid ionization of the NP-DBDs enables rapid gas heating adjacent to the surface, where the plasma layer forms [7]. This gas heating causes a pressure wave to emanate from the discharge region. The pressure wave is initially supersonic but rapidly slows to become an aeroacoustic wave. Roupassov *et al.* [1] first used NP-DBDs for flow application purposes and studied the generation of pressure waves. Since then, several groups have observed pressure waves from volume [8]–[10] and surface discharges [11]–[13].

The use of plasma discharges for flow control is studied here for practical applications in civil and military aircraft or microaerial vehicles. In this context, they must reliably operate over a wide range of environmental conditions, including variable temperature, pressure, humidity, dustiness, and so on. Among these parameters, the pressure has been documented in several papers as having the strongest effect on discharge properties. For instance, a recent numerical simulation of NP-DBD has shown the impact of the near space conditions (pressure of about 50 mbar and temperature of 216 K) on the development of such a discharge [14]. In this paper, the diffuse character of the discharge, the reduction in breakdown voltage, the increase in ion number density, and finally, the reduction in the induced pressure gradient have been clearly revealed. The main conclusion is that the near space conditions leads to energy deposition over a large domain. The result of nonlocalized energy deposition, and then, a heat release distributed over a large surface is a reduction of the pressure wave signature. The influence of pressure has also been investigated in [15] for surface DBD actuators. The influence

Manuscript received June 11, 2015; revised September 11, 2015; accepted February 17, 2016. This work was supported by Labex INTERACTIFS through the French Government Program Investissements d'Avenir under Grant ANR-11-LABX-0017-01.

The authors are with the Centre National de la Recherche Scientifique, École Nationale Supérieure de Mécanique et d'Aérotechnique, Institut Pprime and the Institut Supérieur de l'Aéronautique et de l'Espace, Université de Poitiers, Poitiers 86000, France (e-mail: nicolas.benard@univ-poitiers.fr; kossi.bayoda@univ-poitiers.fr; arthur.aba.a.ndong@univ-poitiers.fr; eric.moreau@univ-poitiers.fr).

Color versions of one or more of the figures in this paper are available online at http://ieeexplore.ieee.org.

Digital Object Identifier 10.1109/TPS.2016.2540160

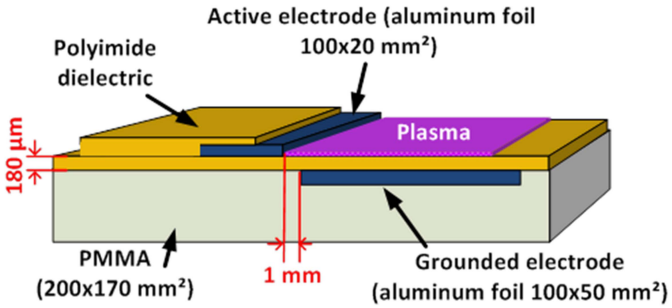

Fig. 1. Schematic of the electrode assembly of the plasma actuator.

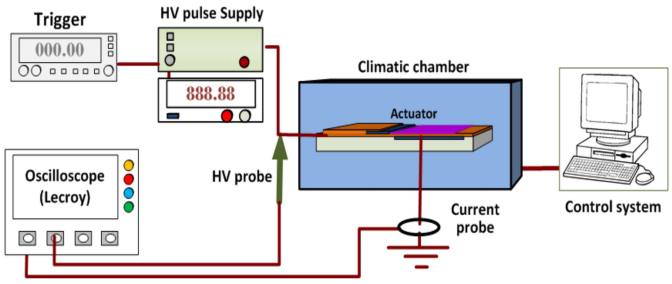

Fig. 2. Schematic of the setup for electrical measurements of the discharge.

of voltage amplitude and frequency has been detailed using ICCD imaging integrated in time. Relevant scaling laws for the plasma layer length, the plasma layer thickness, and the ionization front propagation speed have been defined. For the authors, all these quantities scale with $P^{1/2}$ for a pressure range from 1300 down to 13 mbar.

Here, surface plasma actuators excited by repetitive nanosecond high-voltage pulses are experimentally investigated as a function of ambient pressure (1020–265 mbar), temperature (+20 °C down to −50 °C), or altitude conditions (0–10000 m). Both the electrical characterization and the optical visualization of the discharge are performed in most of the cases, and some complimentary optical visualizations of the induced pressure wave are conducted for varying pressure condition.

II. Experimental Setup

As shown in Fig. 1, the plasma actuator consists of a single DBD mounted on a flat support plate of PMMA (25 mm thick). The electrodes are thin aluminum foils with a thickness of about 80 μm and a span of 100 mm. These electrodes are asymmetrically adhered onto the dielectric layer with a lateral spacing of 1 mm. This dielectric is composed of three layers of polyimide film stuck together with a total thickness of 180 μm. The air-exposed and grounded electrodes are 15 and 44 mm width, respectively. The grounded electrode is encapsulated in epoxy resin to prevent plasma formation on the ground side. The rear and lateral edges of the active electrode are also encapsulated to avoid parasitic discharges, especially at low pressure.

Fig. 2 shows the setup for electrical measurements. High-voltage pulses up to ±10 kV in amplitude are produced

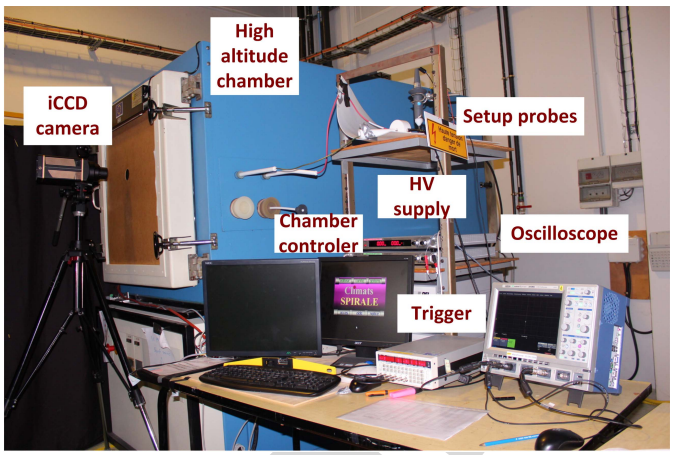

Fig. 3. Image of the altitude chamber, the high-voltage generator, and the intensified CCD camera used for the visualization of the discharge.

by a commercial generator (DEI PVX-4110) powered by a dc power supply (Matsuda, 10P30, 30 mA). The 10%–90% rise time is 70 ns, the duration of maximum voltage is 160 ns, and the fall time is 60 ns. The pulses are triggered by a delay generator (Stanford model DG645). Here, the voltage amplitude is maintained at 10 kV, and pulses are repetitively applied at 10 up to 300 Hz. The measurements presented in this paper concern the 100th pulse applied after switching ON high voltage for each experiment. The current is measured using a passive probe with 400-MHz bandwidth (Bergoz CT-D1.0), and the voltage is measured using a high-voltage passive probe with a bandwidth of 100 MHz and an attenuation ratio of 1000:1 (Lecroy PPE20).

As shown in Fig. 3, a dedicated chamber (Sapratin FCH 350) adjustable both in pressure and temperature is used to reproduce the altitude conditions, as shown in Table I. Its volume is 350 l (790 × 690 × 650 cm^3, for depth, width, and height, respectively). This chamber can reach temperatures from −50 °C to +120 °C, and the pressure can be varied from about 1 down to 0.01 bar. As a result, altitudes from the ground level up to approximately 10 000 m can be reproduced by simultaneously varying pressure and temperature according to Table I.

Optical visualization of the discharge is performed using an intensified CCD camera (Princeton, Pi-Max1 Gen2) with 1024 × 1024 pixel^2 matrix equipped with a 105-mm macrolens. Optical measurements of the pressure wave caused by the local heat release are obtained by a pulsed shadowgraph system that measures the spatial variation of the refractive index via the deflection of light passing through the fluid adjacent to the top electrode. The intensity of light is proportional to the second derivative of the index of refraction. A single head argon-ion laser source (Spectra-Physics 2016, 514 nm) is pulsed by a high-speed shutter gated at 10 kHz. A system of two lenses of 1000 and 600-mm focal length has been used (Fig. 4). Images are collected by an ICCD camera (Pi-Max1) operated with the exposure time of 30 ns. A pulse delay generator (SRS DG645) is used to synchronize measurements with the trigger signal for generating the discharge.

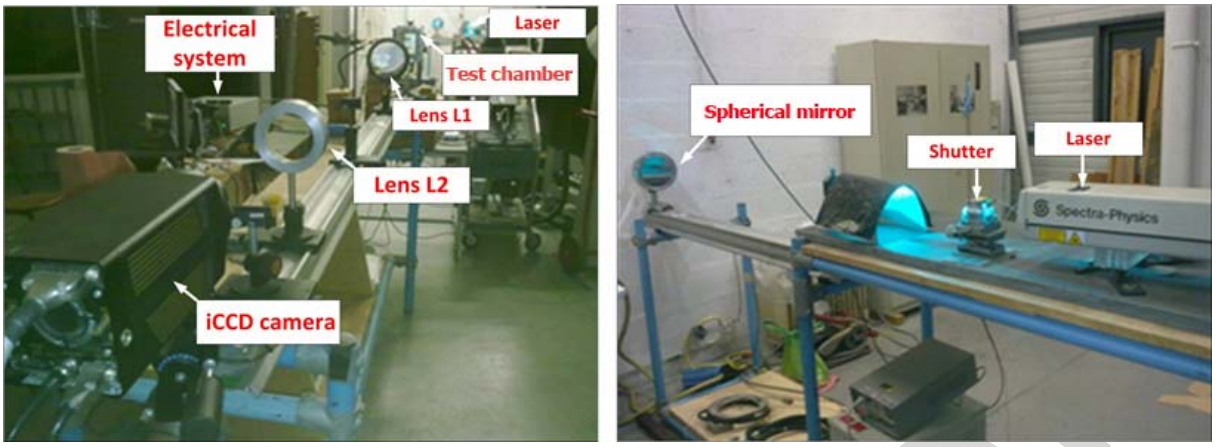

Fig. 4. Photograph of the experimental setup for shadowgraphy images.

TABLE I
PRESSURE AND TEMPERATURE SETTINGS USED TO ACHIEVE DIFFERENT ALTITUDE CONDITIONS

Altitude (m)	Pressure (mbar ou hPa)	Temperature (°C)
0	1020	20
1000	899	8,5
2000	795	2
3000	701	-4,5
4000	616	-11
5000	540	-17,5
6000	472	-24
7000	411	-30,5
8000	356	-37
9000	308	-43,5
10000	265	-50

III. EXPERIMENTAL RESULTS

In this section, we present the experimental results of both discharge and flow characterizations. Our results on discharge characterization are organized into three sections according to the variable of interest, namely, the pressure, temperature, and altitude. This is followed by a discussion on induced pressure wave characterization as a function of pressure only, because the shadowgraph system cannot be easily accommodated with the altitude test chamber.

A. Effect of Pressure on the Discharge Characteristics of NP-DBDs

First, we discuss how the electrical characteristics of the discharge are affected by varying the pressure from 1020 down to 265 mbar with the temperature fixed at 20 °C. Fig. 5 (left) shows the applied voltage and total current waveforms at 1020 and 265 mbar. Note that the total current here is the sum of the capacitive current and the discharge current. The current amplitude increases from 1.1 A/cm at 1020 mbar to 2.3 A/cm at 265 mbar for the current pulse produced during the rise time of the applied voltage. For the current pulse corresponding to the fall time of the applied voltage, the current amplitude increases from −0.7 A/cm at 1020 mbar to −1.5 A/cm at 265 mbar. Like the current amplitude, the time of the formation of the air ionization changes with pressure, because the breakdown voltage decreases with decreasing ambient pressure [14], [16]. We observe a delay in the ignition of the discharge equals to −15 ns when the pressure decreases from 1020 to 265 mbar due to the influence of pressure on the breakdown voltage (5.6 and 4.1 kV at 1020 and 265 mbar, respectively). As expected, the applied voltage maintains the same amplitude at all pressures, but it can be observed that its shape becomes distorted at 265 mbar from its nearly ideal trapezoidal profile at 1020 mbar. This could be caused by the plasma-induced reactance that can alter the discharge circuit.

Fig. 5 (right) shows the power (per-unit length) obtained by multiplying the current and the voltage, as well as the energy obtained by integrating the power in time. The power during the pulse rise time reaches peak values of 11 and 18 kW/cm at 1020 and 265 mbar, respectively. During the fall time of the pulse, the power is much lower, reaching peak values of only 0.1 and 0.15 kW/cm at 1020 and 265 mbar, respectively.

The strength of the pressure wave signature is directly correlated with the discharge energy [7], [12]–[14], this giving motivation for inspecting the changes in the deposited energy. The energy versus time increases up to a maximum value before decreasing to a steady value after the capacitive energy stored in the electrodes has been released during the fall time of the pulse. The final value of the energy increases with decreasing pressure (or increasing air density), as shown in Fig. 6. In this plot, the results for different pulse frequencies are compiled. By reducing the ambient pressure, an increase in the deposited energy is observed. Initially, having a nominal value of 0.47 mJ/cm at 1020 mbar (in agreement with [12] and [13]), the rise in deposited energy reaches up

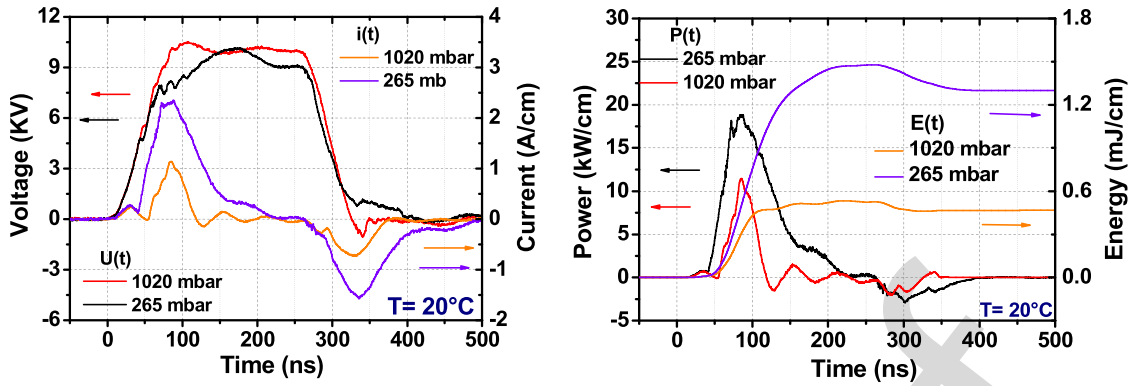

Fig. 5. Measured voltage and current (left) and power per-unit length and energy per-unit length (right) as a function of time at a fixed temperature of 20 °C and two different pressures (pulse frequency of 10 Hz).

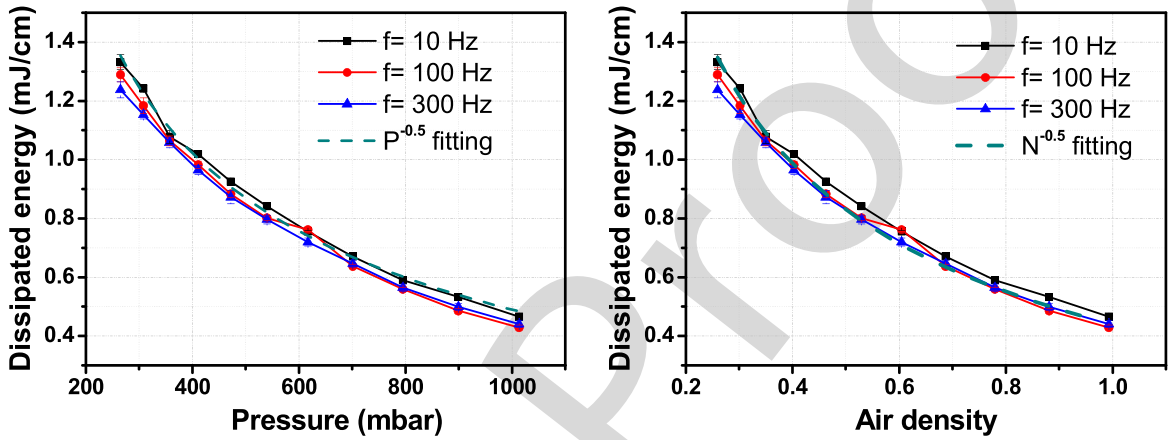

Fig. 6. Measured energy per-unit length as a function of pressure and air density at a fixed temperature of 20 °C.

to 1.16 mJ/cm at 265 mbar. This increase in energy was expected according to the results proposed in [14], and it can be attributed to a reduced breakdown voltage, an increased in charged species mobility, and a higher ion and electron kinetic energies at low pressure. At a given applied voltage, the frequency has almost no influence on the deposited energy in agreement with [15]. As a result, the effect of frequency will not be considered later in this paper.

The dependence of the deposited energy on the pressure over the investigated range can be defined as $U \sim P^{-0.5}$ (where U is the deposited energy and P is the pressure), as proposed in [15]. Another scaling law can be defined in terms of the gas density rather than the ambient pressure. Initially, as proposed in [17], the influence of pressure and temperature on an ac DBD actually simply reflects the changes in gas density in terms of plasma behavior. Here, for instance, the changes in the pressure level produce a reduction in the air density of $-0.75\rho_0$. For the present gas density range and in agreement with the pressure scaling law defined in [15], the empirical relationship $U \sim N^{-0.5}$ is accurate (with N, the gas density).

Next, we discuss how pressure affects the propagation of the discharge. Fig. 7 shows images for two different exposure time intervals that separately show the discharges generated during the rise time [Fig. 7 (phase A)] and the fall time [Fig. 7 (phase B)] of the voltage pulse, for discharges generated at different pressures. During the rise time, the discharge filaments are generally more diffuse in character and more densely spaced along the electrode edge than during the fall time. As the pressure decreases, the discharge extends further during both the rise and fall times due to the increase in mean-free path of electrons. In addition, the discharge length is greater during the fall time at 1020 mbar, but at 265 mbar, there is no more difference in the discharge length between the two intervals.

Single-shot images acquired at a finer time resolution (5 ns) have been used to determine the speed of discharge propagation along the surface, as shown in Fig. 8. During the rise time, we measure the distance traveled by the discharge front from times t_1 to t_2 and then from t_2 to t_3. We then average the two displacements when calculating the speed. The same procedure is used to determine the speed during the fall time using images obtained at times t_4, t_5, and t_6. For both the rise and fall times, the speed of propagation does not vary with pressure to within experimental error. The measured speed is $\sim 0.15 \pm 0.10$ mm/ns. A similar experiment has been conducted in [15]. They report a large dependence of the speed of ionization front propagation with the ambient pressure which is measured to be 0.5–0.7 mm/ns for atmospheric pressure level and increases up to 4 mm/ns at low pressure (13 mbar). Here, the investigated pressure range is probably too small to cause a significant change in ionization speed.

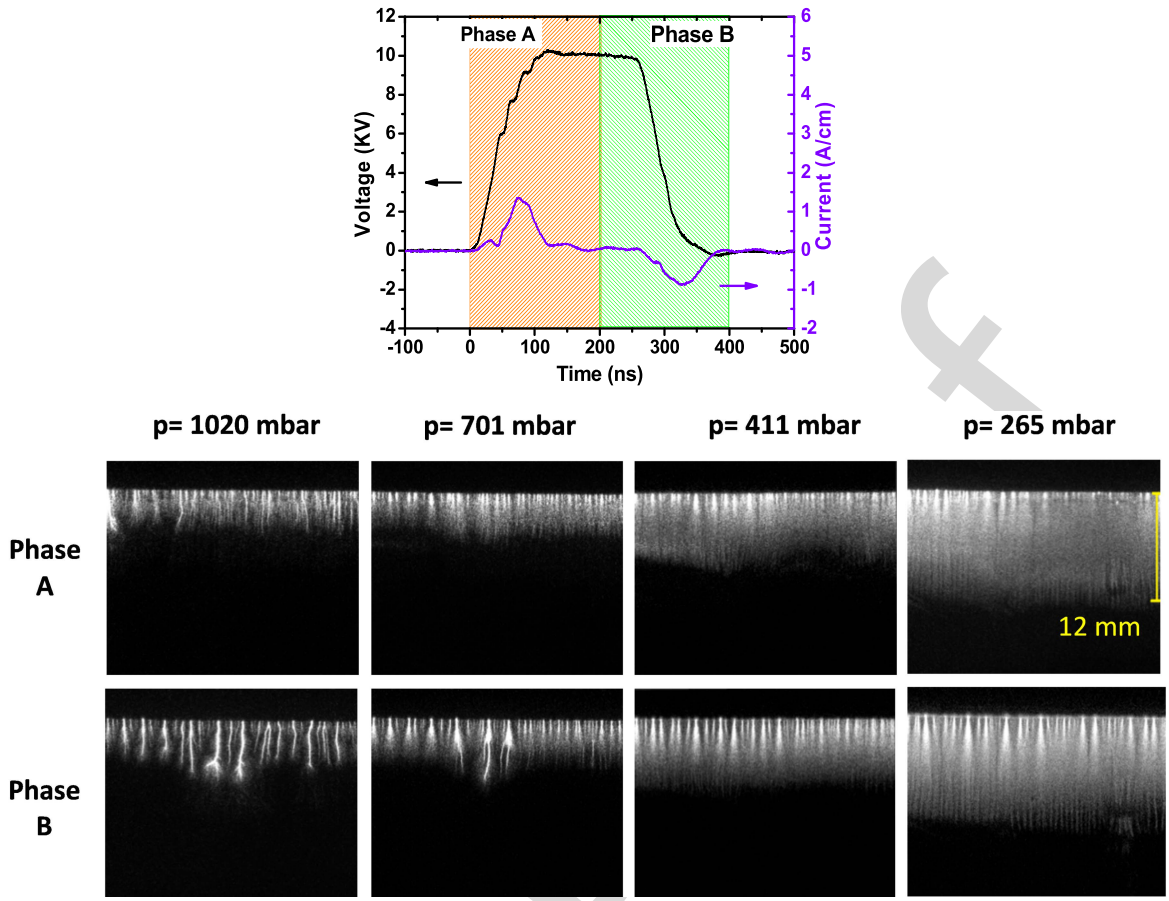

Fig. 7. Exposure time intervals (200 ns) of the intensified CCD camera for single-shot imaging of the discharge during the rise and fall times of the pulse, marked phases A and B (top), and the corresponding top-view images at different pressures (bottom).

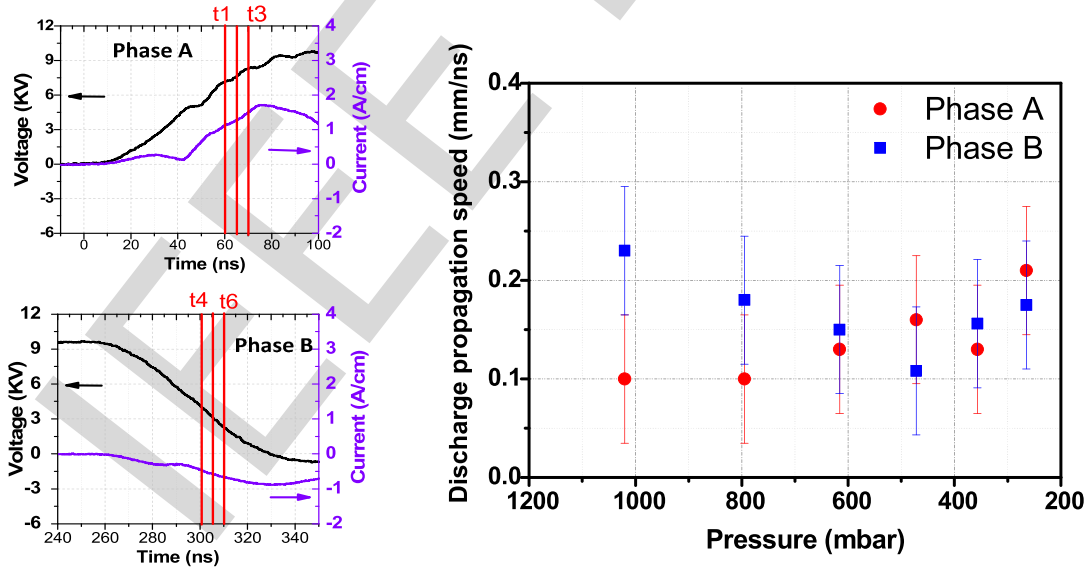

AQ:7 Fig. 8. Times at which single-shot images were acquired using 5-ns exposure times during the rise and fall times of the applied voltage (left) used to calculate the average propagation speed of the discharge during the rise and fall times of the pulse as a function of pressure (right).

B. Effect of Temperature on the Discharge Characteristics of NP-DBDs

Here, we discuss how the electrical characteristics of the discharge are affected by varying the temperature over the range 20 °C to −50 °C with the pressure fixed at 1020 mbar. Fig. 9 (left) shows the current and voltage waveforms obtained at 20 °C and −50 °C. There is almost no change in the amplitude of the current with temperature, but the time of ignition of the current pulse during the rise time of applied voltage appears to be affected. At 20 °C, the current begins to increase above 0 at a time $t = 55$ ns, whereas at −50 °C, the current does not increase until 65 ns. This corroborates

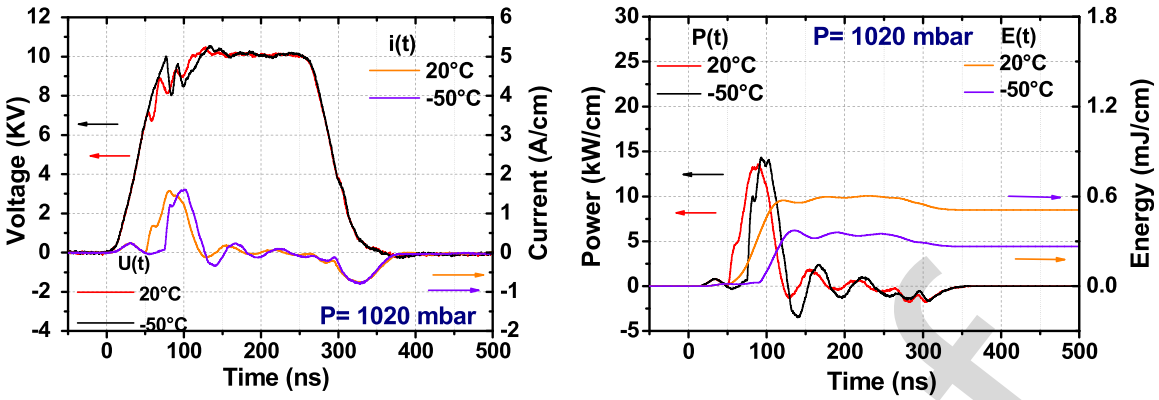

Fig. 9. Measured voltage and current (left) and power and energy (right) as a function of time at a fixed pressure of 1020 mbar and two different temperatures.

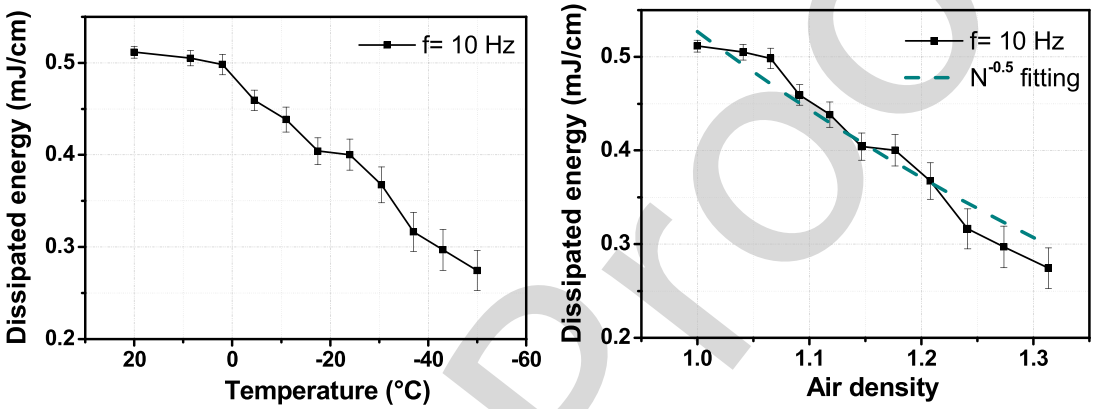

Fig. 10. Dissipated energy per pulse at various temperatures and the corresponding air density (1020 mbar). Values averaged over 100 pulses.

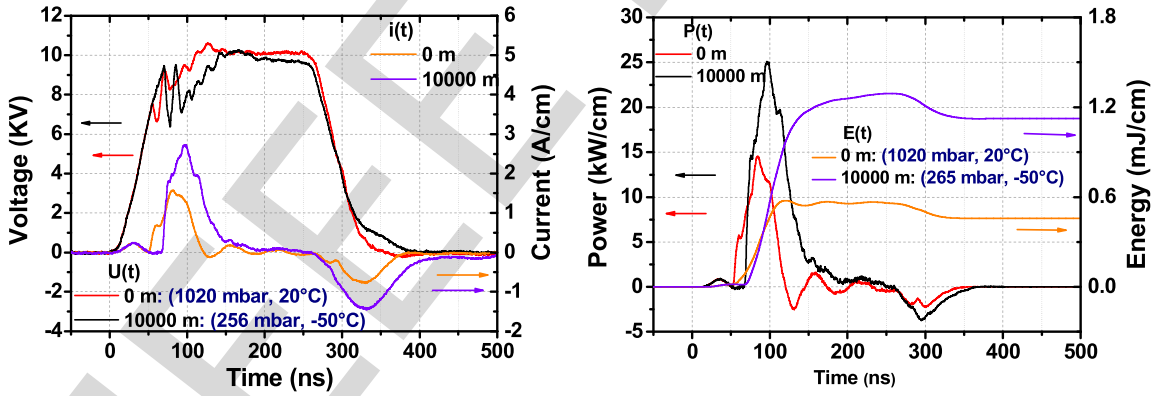

Fig. 11. Measured voltage and current (left) and power and energy (right) as a function of time at altitudes of 0 and 10 km corresponding to temperature and pressures, as shown in Table I.

with an increase in the breakdown voltage at low temperature. However, the negative current peaks form at the same time regardless of the ambient temperature.

Fig. 10 shows how the discharge energy changes with the gas temperature and air density. In general, the energy decreases with the gas temperature, this for the three investigated frequencies. The changes in energy primarily result from the delay observed for the positive current peak. The increase in gas density ($+0.3\rho_0$) promotes reduced mean-free path of charged species. It results lower ion density and a limited extension of the discharge traduces here by a reduction in the deposited energy. If the gas density is considered instead of the temperature, we find that the same empirical relationship $U \sim N^{-0.5}$ found for pressure in Fig. 6 also applies here.

C. Effect of Altitude on the Discharge Characteristics of NP-DBDs

In this section, the influence of the altitude (combined effects of pressure and temperature) is investigated. Fig. 11 shows the current and voltage waveforms for the altitudes of 0 and 10 km. The global behavior of the discharge current

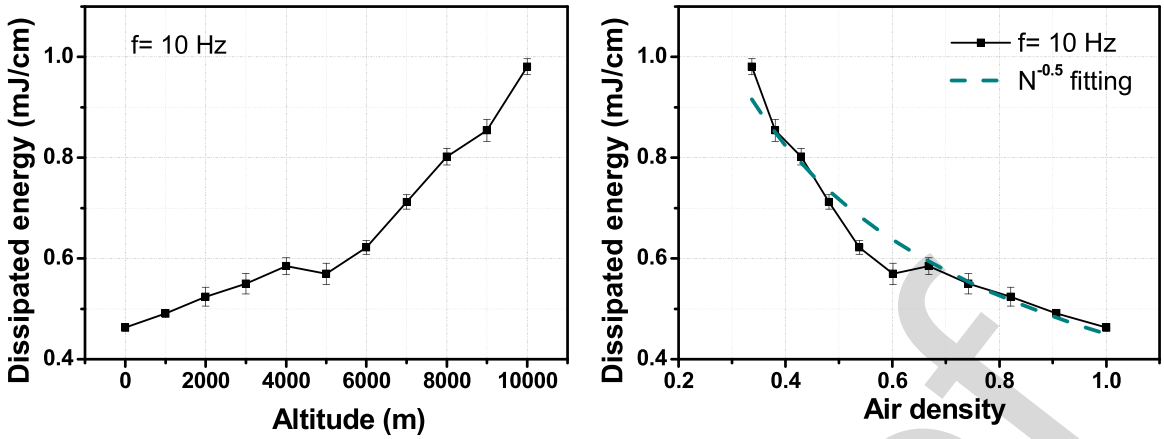

Fig. 12. Dissipated energy by the discharge at various altitude conditions and corresponding air density.

is not strongly modified by the altitude, but a significant increase in the amplitude of both current peaks is observed. The effect of altitude is a mixture of the effects of pressure and temperature. Like the effect of pressure alone shown in Fig. 5, there is a relatively large increase in current amplitude, and the ignition time of the negative current pulse remains unaltered by altitude. However, like the effect of temperature shown in Fig. 9, the ignition time of the positive current pulse is greater at higher altitude suggesting an increased breakdown voltage with altitude. This was not expected as the change in altitude from 0 to 10 km primarily corresponds to air density reduction mainly caused by the change in pressure. Furthermore, past measurements in altitude conditions for ac DBD have shown the domination of pressure on temperature when the altitude increases [16]. Here, the data may deviate from expected results due to the freezing of water vapor, but the power generator may also be incriminated. Indeed, the voltage curves at 10 km shows strong oscillations when the discharge probably develops due to limitation in the capacity of the generator. Fig. 12 shows the effect of altitude and resulting air density on the discharge energy. Like with pressure, a scaling law based on the air density can be defined. The deposited energy scales with $\sim N^{-0.5}$ when the altitude is changed.

Fig. 13 shows the influence of altitude on the deposited energy along with the energy curves in Figs. 6 and 10 (effects of pressure and temperature, respectively). A comparison of the three curves shows that the effect of altitude on discharge energy reflects the changes in gas density. Since the pressure changes over a wider range than the temperature with altitude (i.e., leading to larger changes in air density due to the pressure than due to the temperature), the energy curves as a function of the pressure and altitude are much closer to each other than that as a function of temperature. Overall, the difference in energy between the energy curves as a function of pressure and altitude differs by $18 \pm 8\%$. It is clear that the increase in altitude enhances the energy injected by the NP-DBD. If one considers that a significant part of the injected energy contributes to the local heat deposition, the present results suggest that NP-DBD may have a better effectiveness

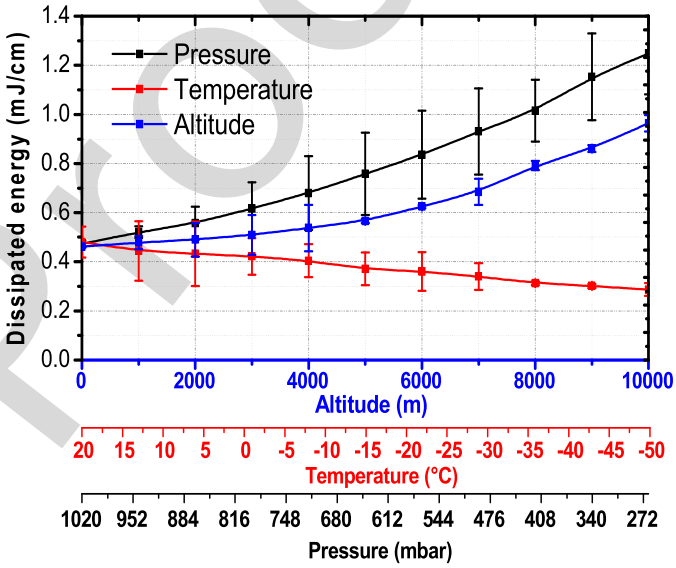

Fig. 13. Dissipated energy as a function of altitude. The energy curves in Figs. 6 and 10 are also shown for comparison.

in realistic flight conditions or sonic flows. However, as numerically demonstrated in [14], the deposited energy at high altitude increases due to a wider and longer plasma region, while the height of the plasma layer is also enlarged at low pressure [15]. These increases positively influence the deposited energy, but the resulting pressure wave is not necessarily reinforced, as the energy deposition is no more localized in a confined region, and a diffuse heat release is promoted instead of a localized one as observed at the ground level.

Like for the pressure, an energy scaling law based on the air density can be defined. All results obtained for pressure, temperature, and altitude are compiled into a single plot by considering the gas density (Fig. 14). Again, the deposited energy matches pretty well with the gas density as $U \sim N^{-0.5}$. This corroborates with the study in [17] (conducted for ac DBD) which suggest that the gas density is the only parameter governing the physics of the discharge. However, as shown in Fig. 14 (zoomed-in view), the results

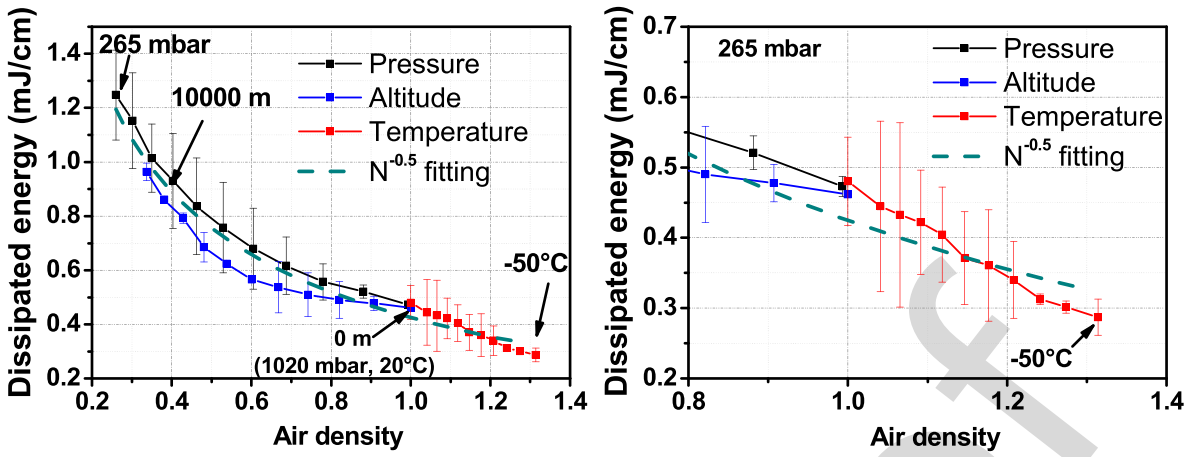

Fig. 14. Compilation of all results plotted according to the air gas density by large (left) and zoomed-in (right) views.

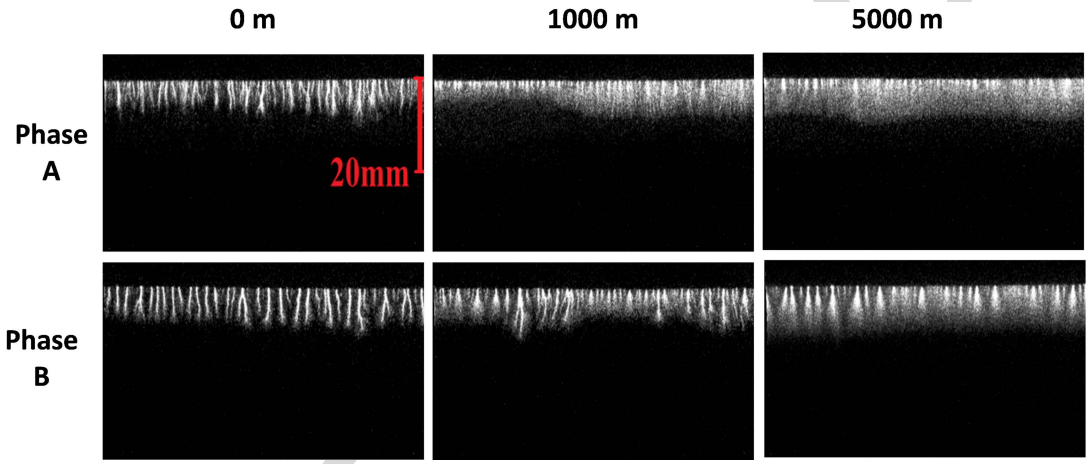

Fig. 15. Top-view images at different altitudes for the same exposure time intervals, as shown in Fig. 7 (200 ns).

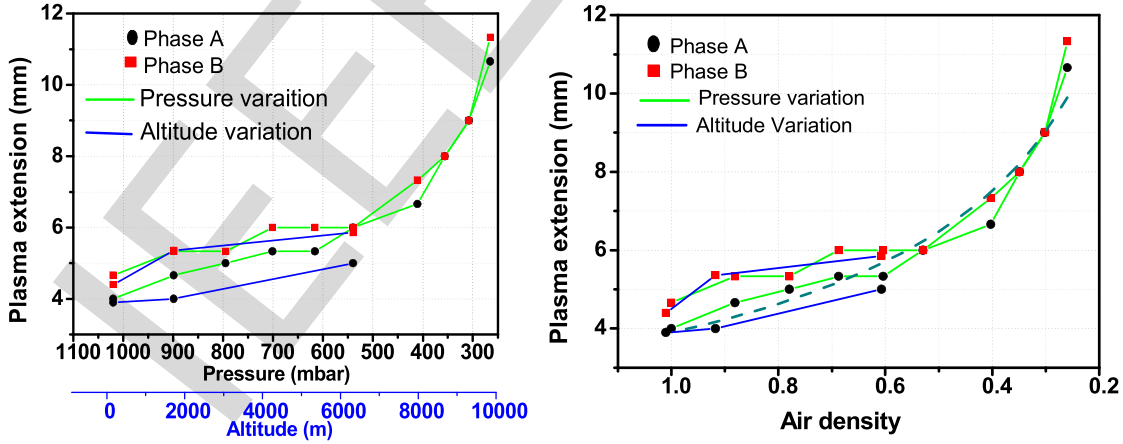

Fig. 16. Discharge extent from the edge of the powered electrode as a function of pressure at a fixed temperature of 20 °C as well as altitude.

deviate from the scaling law $U \sim N^{-0.5}$ at a high gas density, where temperature is negative. It is assumed that this deviation originates from the temperature of the dielectric. Indeed, in addition to the surrounding gas, a change of temperature also influences the permittivity of the dielectric barrier. When the dielectric barrier is at low temperature, its permittivity is reduced leading to a reduction in the dissipated energy, as shown in Fig. 14. It can be concluded that the gas density is a relevant parameter to mimic altitude; however, the influence of temperature on the dielectric is not considered and then this approach is no more valid at low ambient temperature.

Next, we discuss how altitude affects discharge propagation. Fig. 15 shows the images of the discharges generated during the rise and fall times of the pulse for different altitudes using

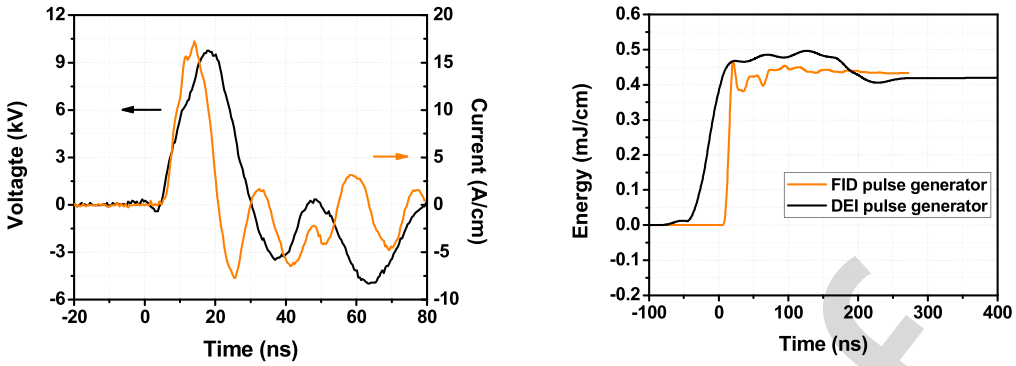

Fig. 17. (a) Voltage and current for an NS-DBD generated by an FID pulse generator. (b) Comparison of the deposited energy for two different pulse generators.

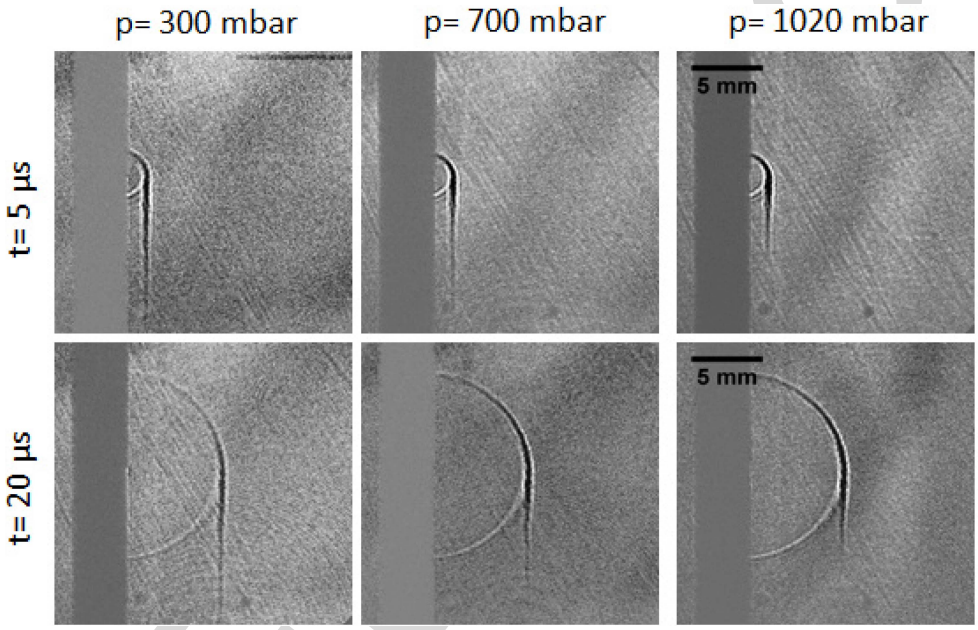

Fig. 18. Shadowgraphy images of the pressure wave generated by discharges excited using the FID generator at different pressures.

the same exposure time intervals, as shown in Fig. 7. Again, during the rise time, the discharge filaments are generally more diffuse in character and more densely spaced along the electrode edge than during the fall time. As the altitude increases, the discharge extends further during both the rise and fall times. Comparison with Fig. 7 shows that the discharge length at a given altitude is about the same as that for the corresponding pressure (see Table I).

Fig. 16 summarizes how the discharge length varies as a function of both pressure and altitude. At altitudes from 0 to 10 km, the variation of discharge length with altitude is very consistent with the effect of pressure, as it was also verified for the deposited energy (Fig. 13). If we consider gas density rather than pressure, the discharge length d thus varies as $d \sim N^{-0.5}$ and the same power law as the energy dependence on gas density, as discussed previously and also the same dependence reported in [15] for pressure variation.

AQ:9 In Section IV, we discuss how the pressure affects shadowgraphy imaging of the flow field, particularly the generation of pressure waves by the discharge. We currently only have shadowgraphy images of pressure waves generated by NP-DBDs using a different high-voltage pulse generator (FID model FPG 40-30NK) than that used for obtaining the previous experimental results. The FID generator produces pulses of 10-ns rise and fall times (see Fig. 17): voltage and current for an NS-DBD generated by an FID pulse generator and comparison of the deposited energy for two different pulse generators. Our purpose here is not to discuss the details of the electrical characteristics of NP-DBDs generated by the FID generator, but rather investigate the change in the pressure wave as a function of the ambient pressure, as shown in Fig. 18. Furthermore, the variation of pressure wave behavior with ambient pressure presented in this section can be considered together with the electrical characteristics studied in the previous sections. Although the experiments were AQ:10 performed using two different high-voltage pulse generators, both generators produce a plasma discharge, whose energy deposition is similar [Fig. 17(b)]. Furthermore, the pressure

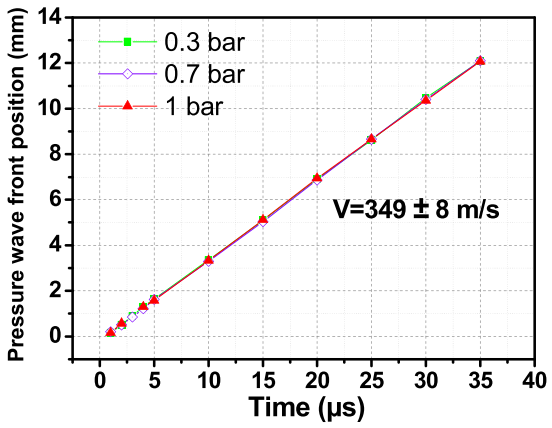

Fig. 19. Propagation speed of the pressure wave for different pressure levels.

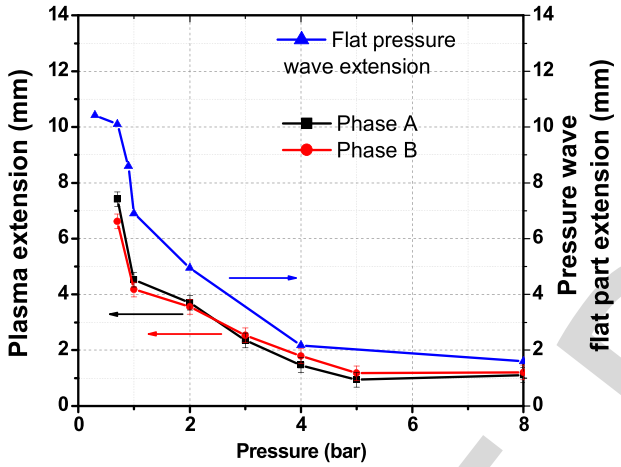

Fig. 20. Plasma layer extension and length of the planar part of the pressure wave at different pressure levels.

dependence is expected to be almost the same in both the cases, because the discharge energy follows the same empirical relationship with gas density, $U \sim N^{-0.5}$, whatever the generator used and the variation of the discharge extension length also follows the same relationship, $d \sim N^{-0.5}$.

The pressure wave is in fact composed of spherical and plane wave components, as observed in the previous experimental [1], [8], [12], [13] or numerical works [14], [18]. The spherical wave is seen to remain rather unchanged with pressure, but the plane wave diminishes in strength and length as the pressure increases from 300 to 1020 mbar. No change in the propagation speed of the pressure wave has been observed over the investigated range of pressure, all propagate at the speed of the sound (∼349 m/s) (Fig. 19). The spherical and plane waves result from rapid volumetric heating close to the electrode edge and along the surface, respectively. Thus, the energy dissipation must vary less with pressure close to the electrode edge than along the surface. Furthermore, as suggested in several papers, such as in [12] or [13], the planar part of the pressure wave results from the heat released during the propagation of filaments on the dielectric barrier surface. This is verified by plotting the plasma extension length together with the length of the planar part of the pressure wave for pressure from 300 mbar to 8 bar (Fig. 20). Both quantities follow the same behavior with close values. This confirms again the good correlation between the length of the planar part of the pressure wave and the extension of the plasma layer, confirming that the planar component of the induced pressure wave is due to the filaments that propagate along the dielectric surface [12].

IV. Conclusion

In this paper, we have investigated the electrical characteristics generated by NP-DBDs in the air, as a function of pressure (265–1020 mbar), temperature (from -50 °C to 20 °C), and altitude (0–10 km). The altitude conditions were reproduced using the appropriate pressure and temperature conditions. We found that the pressure has a much greater effect on plasma characteristics than the temperature. Temperature-specific effects are limited to an increase in the ignition delay time of the discharge with a decreasing temperature, but no significant influence on the discharge was observed. Since the pressure varies much more than the temperature with altitude (and because the change in pressure produces larger changes in gas density than the change in temperature), the changes in discharge characteristics with altitude closely track those of changes in pressure. One important result is that the deposited energy increases with altitude, suggesting that the NP-DBD can be operated at high altitude and probably be effective for flow control. In fact, most of the variations across all the cases can be explained by changes in the gas density rather than independent pressure or temperature effects, in particular, the deposited energy and the plasma extension scale with $N^{-0.5}$. This implies that test chambers where only the gas density can be varied are sufficient to simulate altitude conditions only as a first approximation. However, at low temperature as incurred at high altitude, the permittivity of the dielectric barrier is affected by the environmental conditions and the density matching is no more valid.

The pressure wave issuing from the fast heat release caused by the filaments of the nanosecond discharge has been characterized for low- and high-pressure conditions. In all the cases, a pressure wave propagating at the speed of sound is observed. The primary modifications of the pressure wave topology caused by the pressure relate to an increase in length of the planar part of the wave with increasing pressure. A good correlation is found between the increase of the planar part of the pressure wave and the length of the discharge.

Acknowledgment

The authors would like to thank A. Claverie for the help and fruitful discussions regarding the shadowgraphy method.

References

[1] D. V. Roupassov, A. A. Nikipelov, M. M. Nudnova, and A. Y. Starikovskii, "Flow separation control by plasma actuator with nanosecond pulsed-periodic discharge," *AIAA J.*, vol. 47, no. 1, pp. 168–185, 2009.

[2] J. Little, K. Takashima, M. Nishihara, I. Adamovich, and M. Samimy, "High lift airfoil leading edge separation control with nanosecond pulse DBD plasma actuators," in *Proc. 5th Flow Control Conf. AIAA*, 2010, paper 2010-4256.

[3] C. Rethmel, J. Little, K. Takashima, A. Sinha, I. Adamovich, and M. Samimy, "Flow separation control over an airfoil with nanosecond pulse driven DBD plasma actuators," in *Proc. 49th AIAA Aerosp. Sci. Meeting Including New Horizons Forum Aerosp. Expo.*, 2011, paper 2011-487.

[4] J. Little, K. Takashima, M. Nishihara, I. Adamovich, and M. Samimy, "Separation control with nanosecond-pulse-driven dielectric barrier discharge plasma actuators," *AIAA J.*, vol. 50, no. 2, pp. 350–365, 2012.

[5] I. Popov *et al.*, "Experimental study and numerical simulation of flow separation control with pulsed nanosecond discharge actuator," in *Proc. 51st AIAA Aerosp. Sci. Meeting Including New Horizons Forum Aerosp. Expo.*, 2013, paper 2013-572.

[6] A. Starikovskiy and R. Miles, "Dielectric barrier discharge control and flow acceleration enhancement by diode surface," in *Proc. 51st AIAA Aerosp. Sci. Meeting Including New Horizons Forum Aerosp. Expo.*, 2013, paper 2013-0754.

[7] I. V. Adamovich, J. Little, M. Nishihara, K. Takashima, and M. Samimy, "Nanosecond pulse surface discharges for high-speed flow control," in *Proc. 6th AIAA Flow Control Conf.*, 2012, paper 2012-3137.

[8] B. Arad, Y. Gazit, and A. Ludmirsky, "A sliding discharge device for producing cylindrical shock waves," *J. Phys. D, Appl. Phys.*, vol. 20, no. 3, p. 360, 1987.

[9] R. Ono and T. Oda, "Formation and structure of primary and secondary streamers in positive pulsed corona discharge—Effect of oxygen concentration and applied voltage," *J. Phys. D, Appl. Phys.*, vol. 36, no. 6, p. 1952, Jul. 2003.

[10] D. A. Xu, D. A. Lacoste, D. L. Rusterholtz, P. Q. Elias, G. D. Stancu, and C. O. Laux, "Experimental study of the hydrodynamic expansion following a nanosecond repetitively pulsed discharge in air," *Appl. Phys. Lett.*, vol. 99, no. 12, p. 121502, 2011.

[11] K. Takashima, Y. Zuzeek, W. R. Lempert, and I. V. Adamovich, "Characterization of a surface dielectric barrier discharge plasma sustained by repetitive nanosecond pulses," *Plasma Sour. Sci. Technol.*, vol. 20, no. 5, p. 055009, 2011.

[12] N. Benard, N. Zouzou, A. Claverie, J. Sotton, and E. Moreau, "Optical visualization and electrical characterization of fast-rising pulsed dielectric barrier discharge for airflow control applications," *J. Appl. Phys.*, vol. 111, no. 3, p. 033303, 2012.

[13] R. Dawson and J. Little, "Characterization of nanosecond pulse driven dielectric barrier discharge plasma actuators for aerodynamic flow control," *J. Appl. Phys.*, vol. 113, no. 10, p. 103302, 2013.

[14] X. Che, T. Shao, W. Nie, and P. Yan, "Numerical simulation on a nanosecond-pulse surface dielectric barrier discharge actuator in near space," *J. Phys. D, Appl. Phys.*, vol. 45, no. 14, p. 145201, Mar. 2012.

[15] A. Starikovskiy and S. Pancheshnyi, "Dielectric barrier discharge development at low and moderate pressure conditions," in *Proc. 51st AIAA Aerosp. Sci. Meeting Including New Horizons Forum Aerosp. Expo.*, 2013, paper 2013-0902.

[16] N. Benard and E. Moreau, "Effects of altitude on the electromechanical characteristics of a single dielectric barrier discharge plasma actuator," in *Proc. 41st Plasmadyn. Lasers Conf. AIAA*, 2010, paper 2010-4633.

[17] D. E. Ashpis and D. R. Thurman, "DBD plasma actuators for flow control in air vehicles and jet engines-simulation of flight conditions in test chambers by density matching," in *Proc. 42nd AIAA Plasmadyn. Lasers Conf.*, 2011, paper AIAA-2011-3730.

[18] T. Unfer and J.-P. Boeuf, "Modeling and comparison of sinusoidal and nanosecond pulsed surface dielectric barrier discharges for flow control," *Plasma Phys. Controlled Fusion*, vol. 52, no. 10, p. 124019, Nov. 2010.

Nicolas Benard received the Ph.D. degree in aerodynamic and turbulence from the Université de Poitiers, Poitiers, France, in 2005.

He was an Associate Professor with the Electrical Engineering Department, Université de Poitiers, in 2008. He is a Coordinator of the INOPLAS national research program and was the WP Leader of the MARS EU project. He has authored over 50 full papers in the last six years and participated in about 60 international conferences related to control of laminar and turbulent flows by plasma actuation. His main technical expertise is in development of innovative plasma actuators with interest for their use as flow control devices in open and closed-loop approaches.

Kossi Djidula Bayoda was born in Lomé, Togo, in 1989. He received the M.Sc. degree in energy management from the Université de Poitiers, Poitiers, France, in 2013, where he is currently pursuing the Ph.D. degree in electrical engineering with the Institut Pprime.

His current research interests include nonthermal plasma technology, electrostatic hazards, and active flow control.

Arthur Claude Aba'a Ndong was born in Libreville, Gabon, in 1983. He received the M.Sc. degree in industrial systems engineering and electrical engineering and the Ph.D. degree in electrical engineering from the Université de Poitiers, Poitiers, France, in 2011 and 2014, respectively.

He currently holds a post-doctoral position with the Institut Universitaire de Technologie d'Angoulême, Angoulême, France, where he is involved in particle precipitation and collection by plasma discharge. His current research interests include the applications of electrostatics, nonthermal plasma technology, air pollution control, and electrostatic hazards.

Eric Moreau received the Ph.D. degree in electrical engineering from the Université de Poitiers, Poitiers, France, in 1997.

He became an Assistant Professor with the Université de Poitiers in 1998, where he is currently a Full Professor of Electrical Engineering. He is mainly known for his works on plasma actuators for airflow control, but a part of his research is dedicated to corona-based thrusters and electrostatic precipitation of particles. He has been involved in several European projects, such as CAFEDA, AVERT, OPENAIR, PLASMAERO, MARS, and ORINOCO, and national projects, such as COS, INCA, SINAPS, and INOPLAS. He has authored or co-authored over 100 peer-reviewed articles in international journals and 150 papers in conference proceedings. His current research interests include electrohydrodynamics (EHD), especially the mechanical effects in atmospheric discharges (EHD force, ionic wind, and particle precipitation).

Prof. Moreau is a member of the Advisory Board of the LABEX INTERACTIFS National Grant.

AUTHOR QUERIES

AQ:1 = Please revise the phrase "In the final part" for clarity.
AQ:2 = Please supply index terms/keywords for your paper. To download the IEEE Taxonomy, go to http://www.ieee.org/documents/taxonomy_v101.pdf.
AQ:3 = Please confirm whether the edits made in the current affiliation are OK.
AQ:4 = Please confirm the postal code for "Université de Poitiers."
AQ:5 = Please provide the expansions for the acronyms "ICCD, PMMA, NS, and FID."
AQ:6 = Can the phrase "the authors" be changed to "us?" Please confirm.
AQ:7 = Please confirm whether the edited caption of Fig. 8 is appropriate.
AQ:8 = Please check whether the edits made in the sentence, "This corroborates with the study in [17] …" retain the intended meaning.
AQ:9 = The phrase "In this final part of the paper" has been changed to "In Section IV." Please confirm.
AQ:10 = Please indicate the section numbers for the phrase "the previous sections."
AQ:11 = Please provide the page range for refs. [1], [2], [5]–[7], and [15]–[17].
AQ:12 = Please confirm the retention of the text "His main technical expertise … closed-loop approaches." is OK.
AQ:13 = Current affiliation in biography of "Arthur Claude Aba'a Ndong" does not match First Footnote. Please check.
AQ:14 = Please confirm the retention of the text "He is mainly known for … precipitation of particles." is OK.
AQ:15 = Please confirm whether the edits made in the sentence "His current research interests … precipitation)." are OK.
AQ:16 = Please confirm whether the edits made in the sentence "Prof. Moreau is a member … National Grant." are OK.

A Nanosecond Surface Dielectric Barrier Discharge Operating Under Altitude Conditions for Aeronautics Applications

Nicolas Benard, Kossi Djidula Bayoda, Arthur Claude Aba'a Ndong, and Eric Moreau

***Abstract*— The objective of this paper is to investigate the influence of environmental conditions on a nanosecond pulsed dielectric barrier discharge (NP-DBD). A test chamber where pressure and temperature can be changed to match with realistic altitude conditions has been used. Electrical and optical characterizations of the NP-DBD are proposed for pressure and temperature changes in range related to flow control applications. In particular, the influence of low pressure is investigated. The results indicate that a reduction in pressure leads to a more diffuse plasma layer that further extends with a reducing ambient pressure. The energy dissipated by the discharge increases with a reducing pressure. Regardless of the pressure level, the heat released by the NP-DBD leads to the formation of a pressure wave propagating at sound speed. A good correlation was found between the extension of the plasma layer and the planar part of the produced pressure wave. Similar electrical characterization has been conducted when the temperature is reduced, while the pressure is maintained at an atmospheric level. It was shown that temperature has the minor effect on the discharge characteristics, but lower is the temperature and lower is the deposited energy. In the final part, the influence of the altitude effect is studied by combining pressure and temperature changes. It results that the pressure variation dominates the temperature influence. As a result, higher energy deposition is reported when the altitude is increased. The effect of changes in the pressure and temperature is interpreted as an effect of changes in the gas density. It is concluded that the gas density, N, is an important parameter for studying DBD under the altitude conditions. Indeed, quantities such as the plasma extent and the deposited energy scale with $N^{-0.5}$. However, the gas density does not consider changes in the dielectric permittivity, which restricts the use of the gas density matching method to altitudes with moderate ambient temperature.**

***Index Terms*— XXXXX.**

I. Introduction

PLASMA discharges for flow control have emerged as alternative to mechanical systems over the last decade. Recently, interest has arisen in the use of nanosecond pulsed dielectric barrier discharges (NP-DBDs) for the manipulation of turbulent flows. Originally applied to ozone generation and the destruction of pollutants, these discharges also have a high potential for mitigating separated flows at regimes approaching realistic conditions for applications in aerodynamics [1]–[5]. The current knowledge is not clear regarding the precise effect of this type of discharge. Some authors suggest that the control mechanism is related to the production of vortical flow structures or to interactions between natural vortical flow structures and a local pressure change imposed by the discharge. Another possible reason for the effectiveness of NP-DBDs is its capability to impose the turbulent flow regime in the boundary layer developing the downstream discharge. Unlike typical ac DBDs for which the electric wind is fully responsible for the control mechanism, the NP-DBDs do not produce electric wind [6]. Instead, the rapid ionization of the NP-DBDs enables rapid gas heating adjacent to the surface, where the plasma layer forms [7]. This gas heating causes a pressure wave to emanate from the discharge region. The pressure wave is initially supersonic but rapidly slows to become an aeroacoustic wave. Roupassov *et al.* [1] first used NP-DBDs for flow application purposes and studied the generation of pressure waves. Since then, several groups have observed pressure waves from volume [8]–[10] and surface discharges [11]–[13].

The use of plasma discharges for flow control is studied here for practical applications in civil and military aircraft or microaerial vehicles. In this context, they must reliably operate over a wide range of environmental conditions, including variable temperature, pressure, humidity, dustiness, and so on. Among these parameters, the pressure has been documented in several papers as having the strongest effect on discharge properties. For instance, a recent numerical simulation of NP-DBD has shown the impact of the near space conditions (pressure of about 50 mbar and temperature of 216 K) on the development of such a discharge [14]. In this paper, the diffuse character of the discharge, the reduction in breakdown voltage, the increase in ion number density, and finally, the reduction in the induced pressure gradient have been clearly revealed. The main conclusion is that the near space conditions leads to energy deposition over a large domain. The result of nonlocalized energy deposition, and then, a heat release distributed over a large surface is a reduction of the pressure wave signature. The influence of pressure has also been investigated in [15] for surface DBD actuators. The influence

Manuscript received June 11, 2015; revised September 11, 2015; accepted February 17, 2016. This work was supported by Labex INTERACTIFS through the French Government Program Investissements d'Avenir under Grant ANR-11-LABX-0017-01.

The authors are with the Centre National de la Recherche Scientifique, École Nationale Supérieure de Mécanique et d'Aérotechnique, Institut Pprime and the Institut Supérieur de l'Aéronautique et de l'Espace, Université de Poitiers, Poitiers 86000, France (e-mail: nicolas.benard@univ-poitiers.fr; kossi.bayoda@univ-poitiers.fr; arthur.aba.a.ndong@univ-poitiers.fr; eric.moreau@univ-poitiers.fr).

Color versions of one or more of the figures in this paper are available online at http://ieeexplore.ieee.org.

Digital Object Identifier 10.1109/TPS.2016.2540160

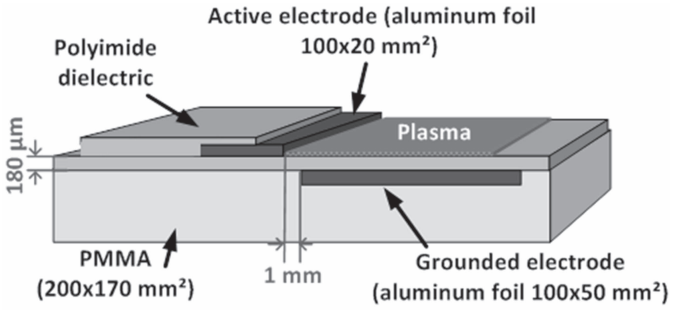

Fig. 1. Schematic of the electrode assembly of the plasma actuator.

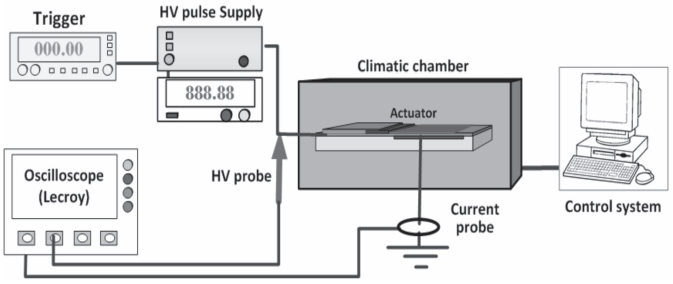

Fig. 2. Schematic of the setup for electrical measurements of the discharge.

of voltage amplitude and frequency has been detailed using ICCD imaging integrated in time. Relevant scaling laws for the plasma layer length, the plasma layer thickness, and the ionization front propagation speed have been defined. For the authors, all these quantities scale with $P^{1/2}$ for a pressure range from 1300 down to 13 mbar.

Here, surface plasma actuators excited by repetitive nanosecond high-voltage pulses are experimentally investigated as a function of ambient pressure (1020–265 mbar), temperature (+20 °C down to −50 °C), or altitude conditions (0–10000 m). Both the electrical characterization and the optical visualization of the discharge are performed in most of the cases, and some complimentary optical visualizations of the induced pressure wave are conducted for varying pressure condition.

II. Experimental Setup

As shown in Fig. 1, the plasma actuator consists of a single DBD mounted on a flat support plate of PMMA (25 mm thick). The electrodes are thin aluminum foils with a thickness of about 80 μm and a span of 100 mm. These electrodes are asymmetrically adhered onto the dielectric layer with a lateral spacing of 1 mm. This dielectric is composed of three layers of polyimide film stuck together with a total thickness of 180 μm. The air-exposed and grounded electrodes are 15 and 44 mm width, respectively. The grounded electrode is encapsulated in epoxy resin to prevent plasma formation on the ground side. The rear and lateral edges of the active electrode are also encapsulated to avoid parasitic discharges, especially at low pressure.

Fig. 2 shows the setup for electrical measurements. High-voltage pulses up to ±10 kV in amplitude are produced by a commercial generator (DEI PVX-4110) powered by a dc power supply (Matsuda, 10P30, 30 mA). The 10%–90% rise time is 70 ns, the duration of maximum voltage is 160 ns, and the fall time is 60 ns. The pulses are triggered by a delay generator (Stanford model DG645). Here, the voltage amplitude is maintained at 10 kV, and pulses are repetitively applied at 10 up to 300 Hz. The measurements presented in this paper concern the 100th pulse applied after switching ON high voltage for each experiment. The current is measured using a passive probe with 400-MHz bandwidth (Bergoz CT-D1.0), and the voltage is measured using a high-voltage passive probe with a bandwidth of 100 MHz and an attenuation ratio of 1000:1 (Lecroy PPE20).

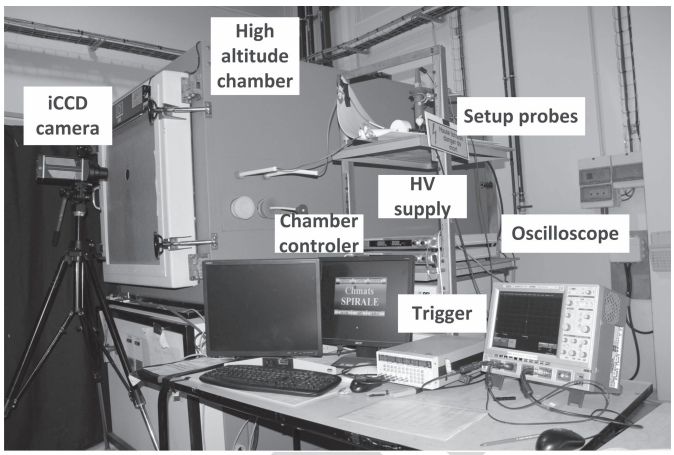

Fig. 3. Image of the altitude chamber, the high-voltage generator, and the intensified CCD camera used for the visualization of the discharge.

As shown in Fig. 3, a dedicated chamber (Sapratin FCH 350) adjustable both in pressure and temperature is used to reproduce the altitude conditions, as shown in Table I. Its volume is 350 l (790 × 690 × 650 cm^3, for depth, width, and height, respectively). This chamber can reach temperatures from −50 °C to +120 °C, and the pressure can be varied from about 1 down to 0.01 bar. As a result, altitudes from the ground level up to approximately 10 000 m can be reproduced by simultaneously varying pressure and temperature according to Table I.

Optical visualization of the discharge is performed using an intensified CCD camera (Princeton, Pi-Max1 Gen2) with 1024×1024 pixel^2 matrix equipped with a 105-mm macrolens. Optical measurements of the pressure wave caused by the local heat release are obtained by a pulsed shadowgraph system that measures the spatial variation of the refractive index via the deflection of light passing through the fluid adjacent to the top electrode. The intensity of light is proportional to the second derivative of the index of refraction. A single head argon-ion laser source (Spectra-Physics 2016, 514 nm) is pulsed by a high-speed shutter gated at 10 kHz. A system of two lenses of 1000 and 600-mm focal length has been used (Fig. 4). Images are collected by an ICCD camera (Pi-Max1) operated with the exposure time of 30 ns. A pulse delay generator (SRS DG645) is used to synchronize measurements with the trigger signal for generating the discharge.

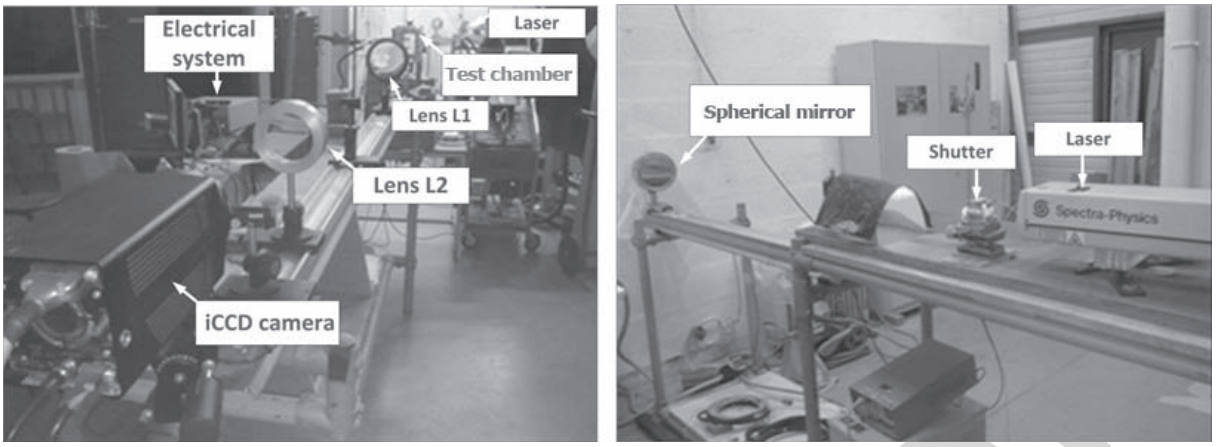

Fig. 4. Photograph of the experimental setup for shadowgraphy images.

TABLE I
PRESSURE AND TEMPERATURE SETTINGS USED TO ACHIEVE DIFFERENT ALTITUDE CONDITIONS

Altitude (m)	Pressure (mbar ou hPa)	Temperature (°C)
0	1020	20
1000	899	8,5
2000	795	2
3000	701	-4,5
4000	616	-11
5000	540	-17,5
6000	472	-24
7000	411	-30,5
8000	356	-37
9000	308	-43,5
10000	265	-50

III. EXPERIMENTAL RESULTS

In this section, we present the experimental results of both discharge and flow characterizations. Our results on discharge characterization are organized into three sections according to the variable of interest, namely, the pressure, temperature, and altitude. This is followed by a discussion on induced pressure wave characterization as a function of pressure only, because the shadowgraph system cannot be easily accommodated with the altitude test chamber.

A. Effect of Pressure on the Discharge Characteristics of NP-DBDs

First, we discuss how the electrical characteristics of the discharge are affected by varying the pressure from 1020 down to 265 mbar with the temperature fixed at 20 °C. Fig. 5 (left) shows the applied voltage and total current waveforms at 1020 and 265 mbar. Note that the total current here is the sum of the capacitive current and the discharge current. The current amplitude increases from 1.1 A/cm at 1020 mbar to 2.3 A/cm at 265 mbar for the current pulse produced during the rise time of the applied voltage. For the current pulse corresponding to the fall time of the applied voltage, the current amplitude increases from −0.7 A/cm at 1020 mbar to −1.5 A/cm at 265 mbar. Like the current amplitude, the time of the formation of the air ionization changes with pressure, because the breakdown voltage decreases with decreasing ambient pressure [14], [16]. We observe a delay in the ignition of the discharge equals to −15 ns when the pressure decreases from 1020 to 265 mbar due to the influence of pressure on the breakdown voltage (5.6 and 4.1 kV at 1020 and 265 mbar, respectively). As expected, the applied voltage maintains the same amplitude at all pressures, but it can be observed that its shape becomes distorted at 265 mbar from its nearly ideal trapezoidal profile at 1020 mbar. This could be caused by the plasma-induced reactance that can alter the discharge circuit.

Fig. 5 (right) shows the power (per-unit length) obtained by multiplying the current and the voltage, as well as the energy obtained by integrating the power in time. The power during the pulse rise time reaches peak values of 11 and 18 kW/cm at 1020 and 265 mbar, respectively. During the fall time of the pulse, the power is much lower, reaching peak values of only 0.1 and 0.15 kW/cm at 1020 and 265 mbar, respectively.

The strength of the pressure wave signature is directly correlated with the discharge energy [7], [12]–[14], this giving motivation for inspecting the changes in the deposited energy. The energy versus time increases up to a maximum value before decreasing to a steady value after the capacitive energy stored in the electrodes has been released during the fall time of the pulse. The final value of the energy increases with decreasing pressure (or increasing air density), as shown in Fig. 6. In this plot, the results for different pulse frequencies are compiled. By reducing the ambient pressure, an increase in the deposited energy is observed. Initially, having a nominal value of 0.47 mJ/cm at 1020 mbar (in agreement with [12] and [13]), the rise in deposited energy reaches up

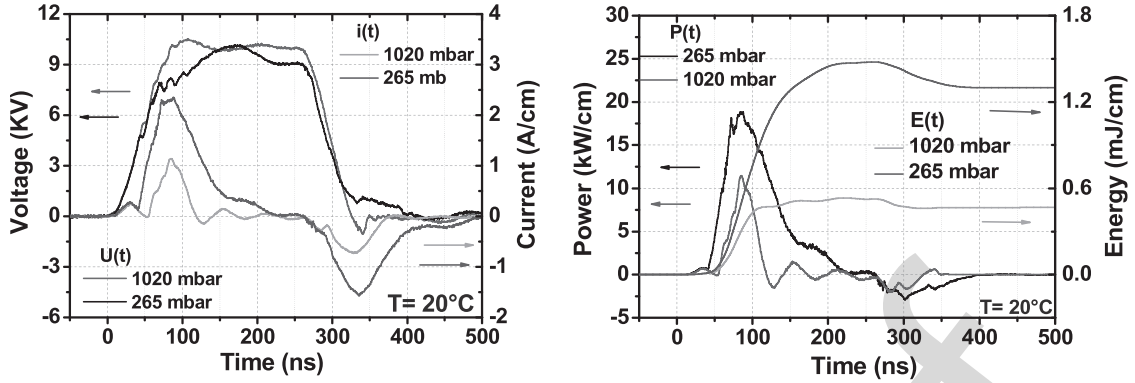

Fig. 5. Measured voltage and current (left) and power per-unit length and energy per-unit length (right) as a function of time at a fixed temperature of 20 °C and two different pressures (pulse frequency of 10 Hz).

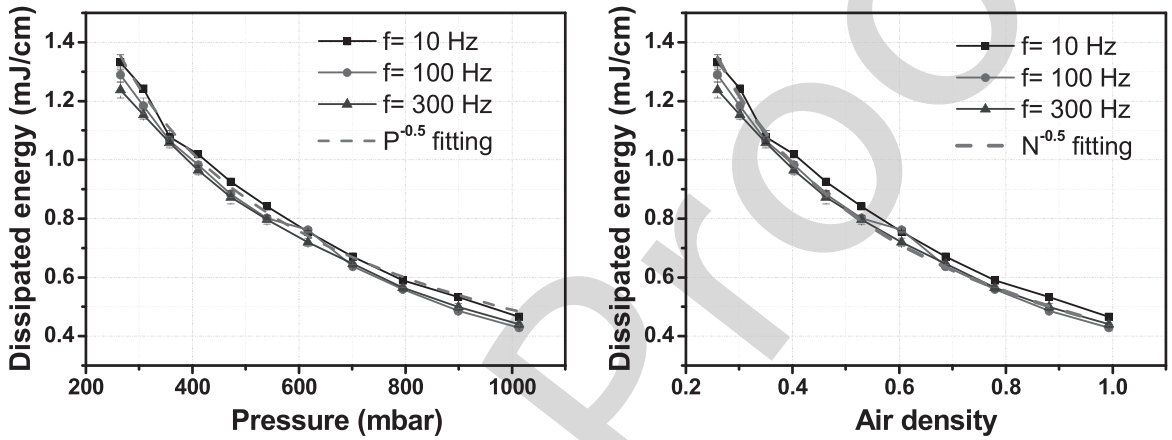

Fig. 6. Measured energy per-unit length as a function of pressure and air density at a fixed temperature of 20 °C.

to 1.16 mJ/cm at 265 mbar. This increase in energy was expected according to the results proposed in [14], and it can be attributed to a reduced breakdown voltage, an increased in charged species mobility, and a higher ion and electron kinetic energies at low pressure. At a given applied voltage, the frequency has almost no influence on the deposited energy in agreement with [15]. As a result, the effect of frequency will not be considered later in this paper.

The dependence of the deposited energy on the pressure over the investigated range can be defined as $U \sim P^{-0.5}$ (where U is the deposited energy and P is the pressure), as proposed in [15]. Another scaling law can be defined in terms of the gas density rather than the ambient pressure. Initially, as proposed in [17], the influence of pressure and temperature on an ac DBD actually simply reflects the changes in gas density in terms of plasma behavior. Here, for instance, the changes in the pressure level produce a reduction in the air density of $-0.75\rho_0$. For the present gas density range and in agreement with the pressure scaling law defined in [15], the empirical relationship $U \sim N^{-0.5}$ is accurate (with N, the gas density).

Next, we discuss how pressure affects the propagation of the discharge. Fig. 7 shows images for two different exposure time intervals that separately show the discharges generated during the rise time [Fig. 7 (phase A)] and the fall time [Fig. 7 (phase B)] of the voltage pulse, for discharges generated at different pressures. During the rise time, the discharge filaments are generally more diffuse in character and more densely spaced along the electrode edge than during the fall time. As the pressure decreases, the discharge extends further during both the rise and fall times due to the increase in mean-free path of electrons. In addition, the discharge length is greater during the fall time at 1020 mbar, but at 265 mbar, there is no more difference in the discharge length between the two intervals.

Single-shot images acquired at a finer time resolution (5 ns) have been used to determine the speed of discharge propagation along the surface, as shown in Fig. 8. During the rise time, we measure the distance traveled by the discharge front from times t_1 to t_2 and then from t_2 to t_3. We then average the two displacements when calculating the speed. The same procedure is used to determine the speed during the fall time using images obtained at times t_4, t_5, and t_6. For both the rise and fall times, the speed of propagation does not vary with pressure to within experimental error. The measured speed is $\sim 0.15 \pm 0.10$ mm/ns. A similar experiment has been conducted in [15]. They report a large dependence of the speed of ionization front propagation with the ambient pressure which is measured to be 0.5–0.7 mm/ns for atmospheric pressure level and increases up to 4 mm/ns at low pressure (13 mbar). Here, the investigated pressure range is probably too small to cause a significant change in ionization speed.

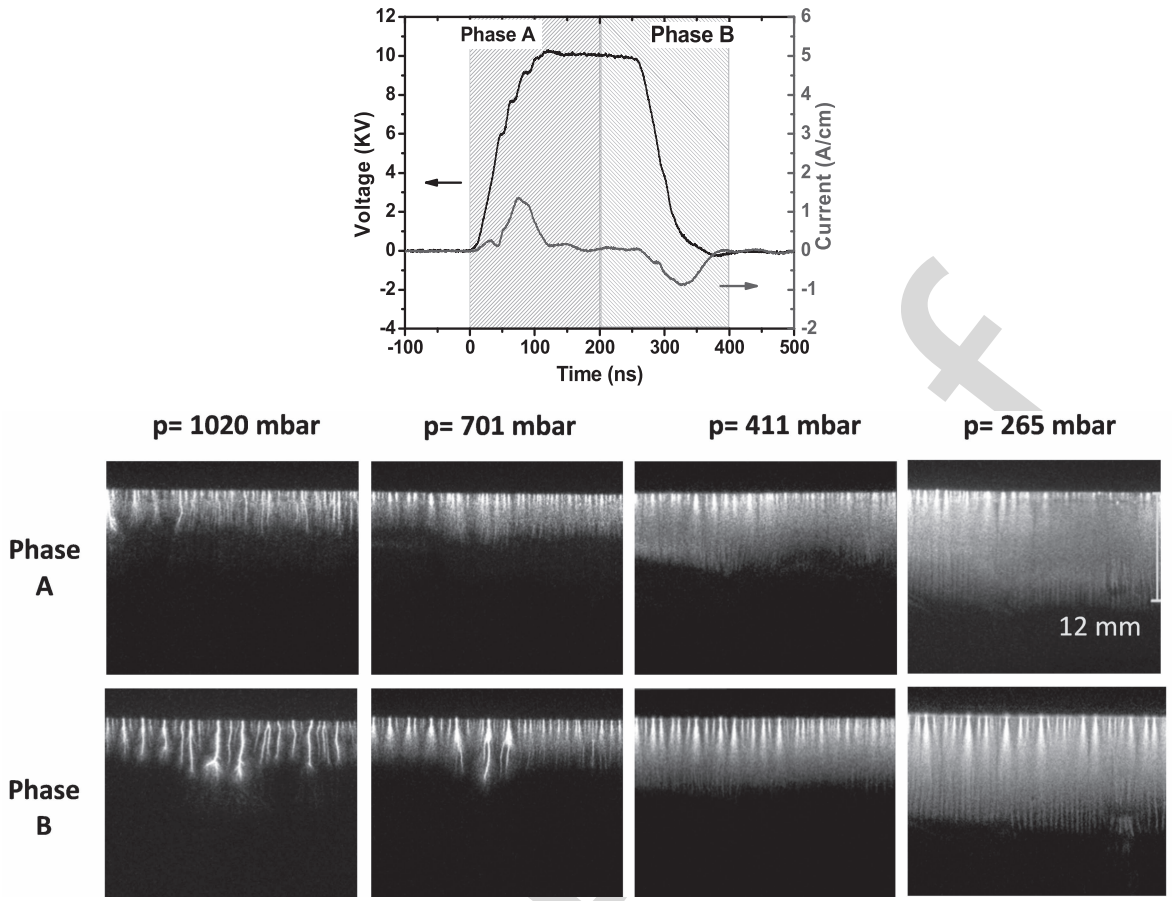

Fig. 7. Exposure time intervals (200 ns) of the intensified CCD camera for single-shot imaging of the discharge during the rise and fall times of the pulse, marked phases A and B (top), and the corresponding top-view images at different pressures (bottom).

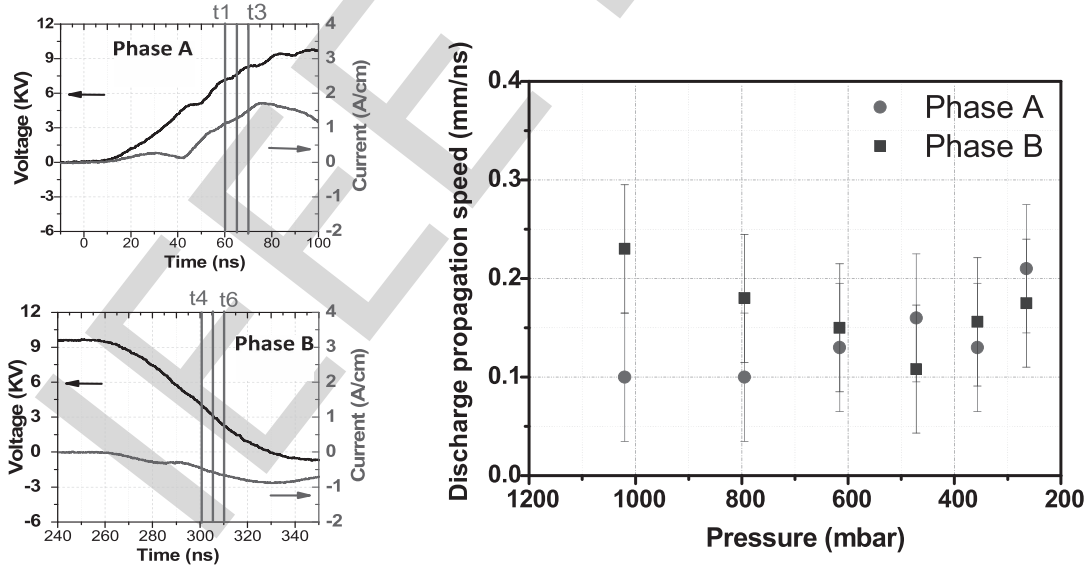

Fig. 8. Times at which single-shot images were acquired using 5-ns exposure times during the rise and fall times of the applied voltage (left) used to calculate the average propagation speed of the discharge during the rise and fall times of the pulse as a function of pressure (right).

B. Effect of Temperature on the Discharge Characteristics of NP-DBDs

Here, we discuss how the electrical characteristics of the discharge are affected by varying the temperature over the range 20 °C to −50 °C with the pressure fixed at 1020 mbar. Fig. 9 (left) shows the current and voltage waveforms obtained at 20 °C and −50 °C. There is almost no change in the amplitude of the current with temperature, but the time of ignition of the current pulse during the rise time of applied voltage appears to be affected. At 20 °C, the current begins to increase above 0 at a time $t = 55$ ns, whereas at −50 °C, the current does not increase until 65 ns. This corroborates

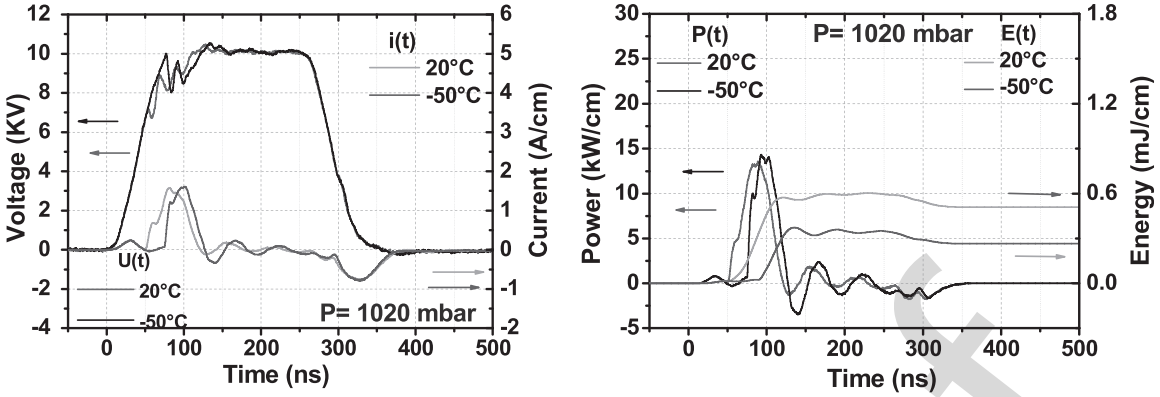

Fig. 9. Measured voltage and current (left) and power and energy (right) as a function of time at a fixed pressure of 1020 mbar and two different temperatures.

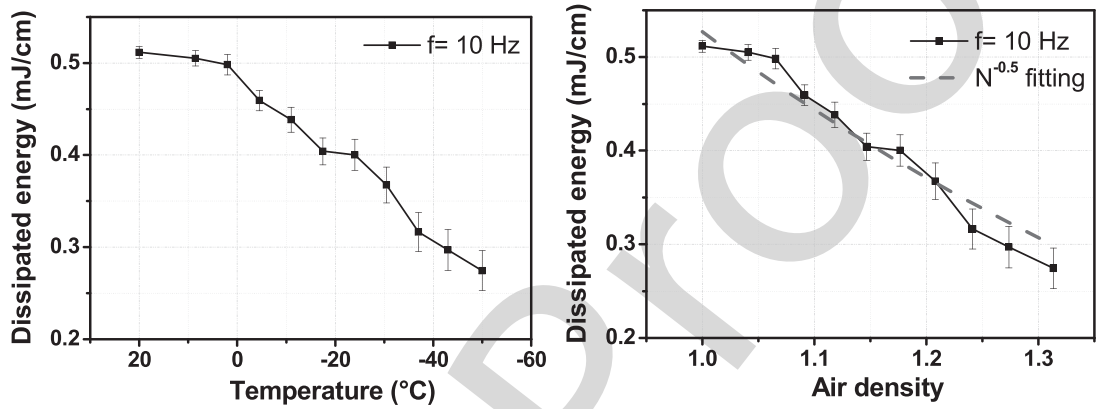

Fig. 10. Dissipated energy per pulse at various temperatures and the corresponding air density (1020 mbar). Values averaged over 100 pulses.

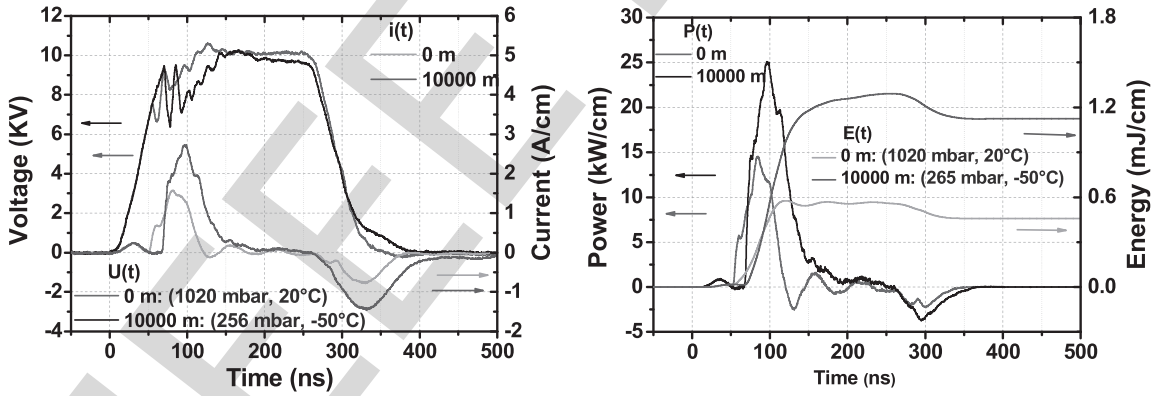

Fig. 11. Measured voltage and current (left) and power and energy (right) as a function of time at altitudes of 0 and 10 km corresponding to temperature and pressures, as shown in Table I.

with an increase in the breakdown voltage at low temperature. However, the negative current peaks form at the same time regardless of the ambient temperature.

Fig. 10 shows how the discharge energy changes with the gas temperature and air density. In general, the energy decreases with the gas temperature, this for the three investigated frequencies. The changes in energy primarily result from the delay observed for the positive current peak. The increase in gas density ($+0.3\rho_0$) promotes reduced mean-free path of charged species. It results lower ion density and a limited extension of the discharge traduces here by a reduction in the deposited energy. If the gas density is considered instead of the temperature, we find that the same empirical relationship $U \sim N^{-0.5}$ found for pressure in Fig. 6 also applies here.

C. Effect of Altitude on the Discharge Characteristics of NP-DBDs

In this section, the influence of the altitude (combined effects of pressure and temperature) is investigated. Fig. 11 shows the current and voltage waveforms for the altitudes of 0 and 10 km. The global behavior of the discharge current

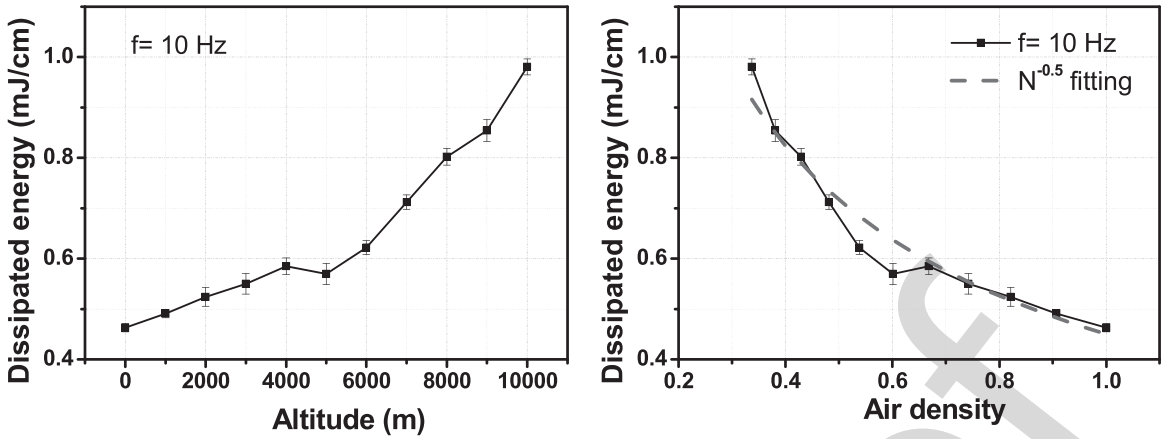

Fig. 12. Dissipated energy by the discharge at various altitude conditions and corresponding air density.

is not strongly modified by the altitude, but a significant increase in the amplitude of both current peaks is observed. The effect of altitude is a mixture of the effects of pressure and temperature. Like the effect of pressure alone shown in Fig. 5, there is a relatively large increase in current amplitude, and the ignition time of the negative current pulse remains unaltered by altitude. However, like the effect of temperature shown in Fig. 9, the ignition time of the positive current pulse is greater at higher altitude suggesting an increased breakdown voltage with altitude. This was not expected as the change in altitude from 0 to 10 km primarily corresponds to air density reduction mainly caused by the change in pressure. Furthermore, past measurements in altitude conditions for ac DBD have shown the domination of pressure on temperature when the altitude increases [16]. Here, the data may deviate from expected results due to the freezing of water vapor, but the power generator may also be incriminated. Indeed, the voltage curves at 10 km shows strong oscillations when the discharge probably develops due to limitation in the capacity of the generator. Fig. 12 shows the effect of altitude and resulting air density on the discharge energy. Like with pressure, a scaling law based on the air density can be defined. The deposited energy scales with $\sim N^{-0.5}$ when the altitude is changed.

Fig. 13 shows the influence of altitude on the deposited energy along with the energy curves in Figs. 6 and 10 (effects of pressure and temperature, respectively). A comparison of the three curves shows that the effect of altitude on discharge energy reflects the changes in gas density. Since the pressure changes over a wider range than the temperature with altitude (i.e., leading to larger changes in air density due to the pressure than due to the temperature), the energy curves as a function of the pressure and altitude are much closer to each other than that as a function of temperature. Overall, the difference in energy between the energy curves as a function of pressure and altitude differs by $18 \pm 8\%$. It is clear that the increase in altitude enhances the energy injected by the NP-DBD. If one considers that a significant part of the injected energy contributes to the local heat deposition, the present results suggest that NP-DBD may have a better effectiveness

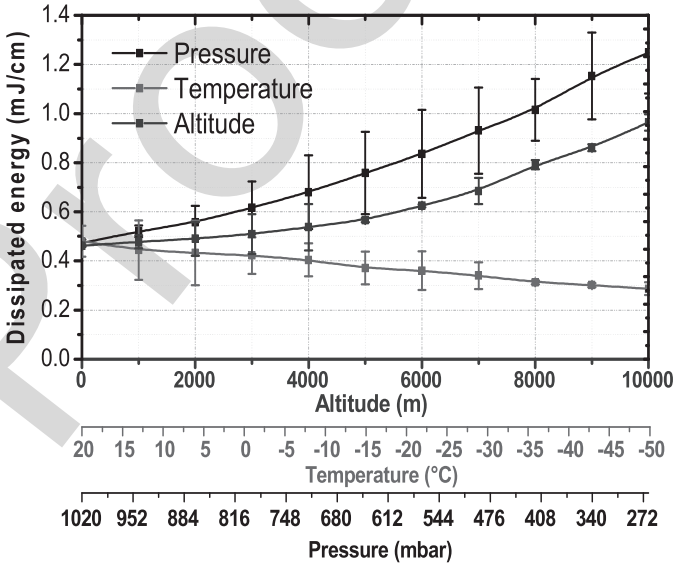

Fig. 13. Dissipated energy as a function of altitude. The energy curves in Figs. 6 and 10 are also shown for comparison.

in realistic flight conditions or sonic flows. However, as numerically demonstrated in [14], the deposited energy at high altitude increases due to a wider and longer plasma region, while the height of the plasma layer is also enlarged at low pressure [15]. These increases positively influence the deposited energy, but the resulting pressure wave is not necessarily reinforced, as the energy deposition is no more localized in a confined region, and a diffuse heat release is promoted instead of a localized one as observed at the ground level.

Like for the pressure, an energy scaling law based on the air density can be defined. All results obtained for pressure, temperature, and altitude are compiled into a single plot by considering the gas density (Fig. 14). Again, the deposited energy matches pretty well with the gas density as $U \sim N^{-0.5}$. This corroborates with the study in [17] (conducted for ac DBD) which suggest that the gas density is the only parameter governing the physics of the discharge. However, as shown in Fig. 14 (zoomed-in view), the results

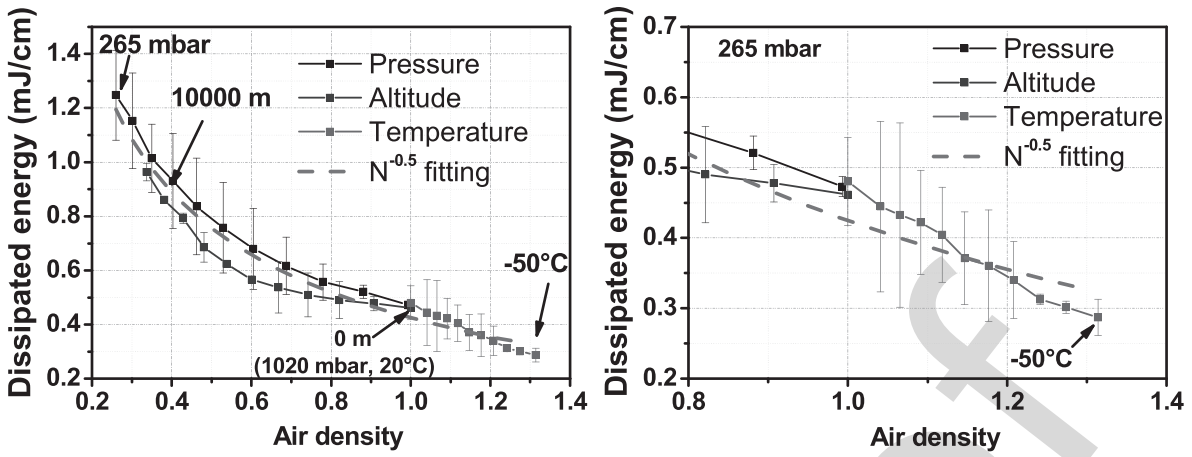

Fig. 14. Compilation of all results plotted according to the air gas density by large (left) and zoomed-in (right) views.

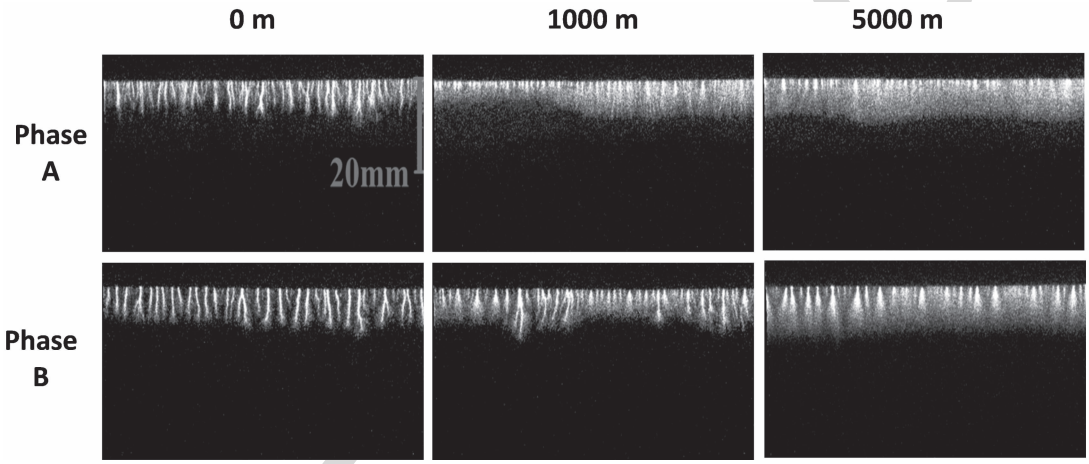

Fig. 15. Top-view images at different altitudes for the same exposure time intervals, as shown in Fig. 7 (200 ns).

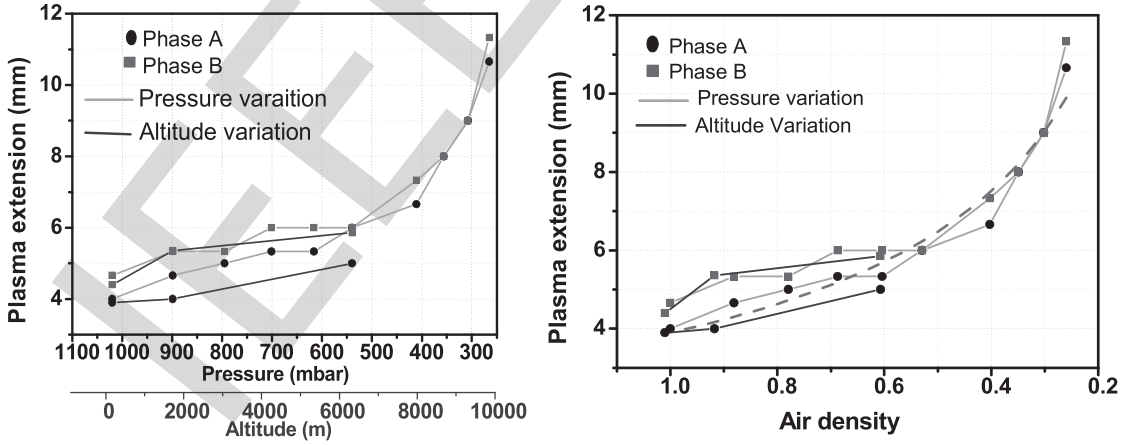

Fig. 16. Discharge extent from the edge of the powered electrode as a function of pressure at a fixed temperature of 20 °C as well as altitude.

deviate from the scaling law $U \sim N^{-0.5}$ at a high gas density, where temperature is negative. It is assumed that this deviation originates from the temperature of the dielectric. Indeed, in addition to the surrounding gas, a change of temperature also influences the permittivity of the dielectric barrier. When the dielectric barrier is at low temperature, its permittivity is reduced leading to a reduction in the dissipated energy, as shown in Fig. 14. It can be concluded that the gas density is a relevant parameter to mimic altitude; however, the influence of temperature on the dielectric is not considered and then this approach is no more valid at low ambient temperature.

Next, we discuss how altitude affects discharge propagation. Fig. 15 shows the images of the discharges generated during the rise and fall times of the pulse for different altitudes using

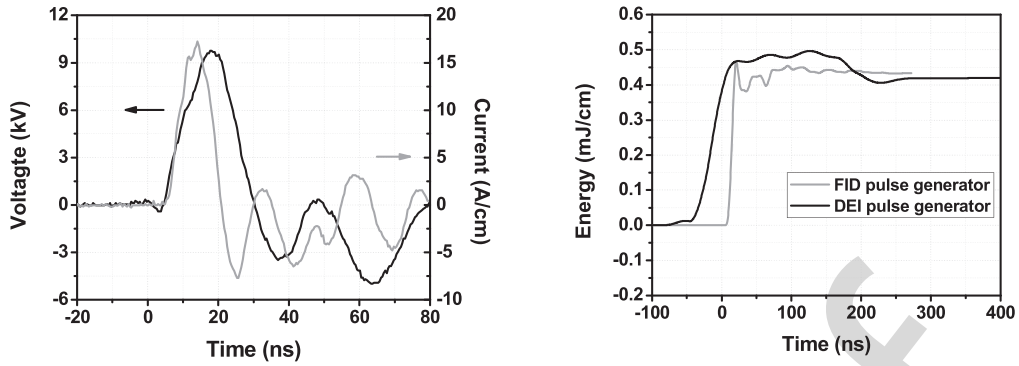

Fig. 17. (a) Voltage and current for an NS-DBD generated by an FID pulse generator. (b) Comparison of the deposited energy for two different pulse generators.

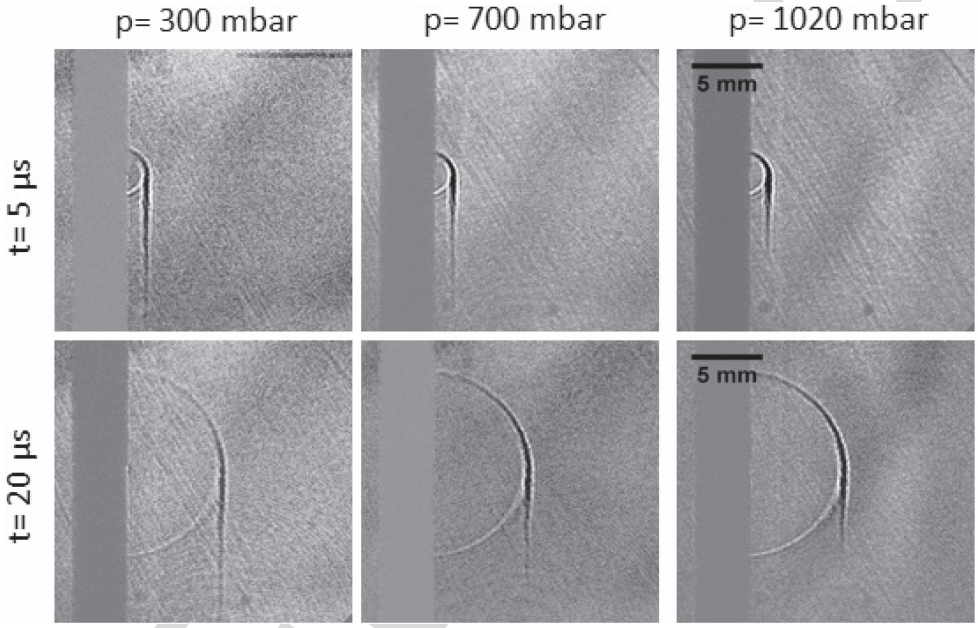

Fig. 18. Shadowgraphy images of the pressure wave generated by discharges excited using the FID generator at different pressures.

the same exposure time intervals, as shown in Fig. 7. Again, during the rise time, the discharge filaments are generally more diffuse in character and more densely spaced along the electrode edge than during the fall time. As the altitude increases, the discharge extends further during both the rise and fall times. Comparison with Fig. 7 shows that the discharge length at a given altitude is about the same as that for the corresponding pressure (see Table I).

Fig. 16 summarizes how the discharge length varies as a function of both pressure and altitude. At altitudes from 0 to 10 km, the variation of discharge length with altitude is very consistent with the effect of pressure, as it was also verified for the deposited energy (Fig. 13). If we consider gas density rather than pressure, the discharge length d thus varies as $d \sim N^{-0.5}$ and the same power law as the energy dependence on gas density, as discussed previously and also the same dependence reported in [15] for pressure variation.

AQ:9 In Section IV, we discuss how the pressure affects shadowgraphy imaging of the flow field, particularly the generation of pressure waves by the discharge. We currently only have shadowgraphy images of pressure waves generated by NP-DBDs using a different high-voltage pulse generator (FID model FPG 40-30NK) than that used for obtaining the previous experimental results. The FID generator produces pulses of 10-ns rise and fall times (see Fig. 17): voltage and current for an NS-DBD generated by an FID pulse generator and comparison of the deposited energy for two different pulse generators. Our purpose here is not to discuss the details of the electrical characteristics of NP-DBDs generated by the FID generator, but rather investigate the change in the pressure wave as a function of the ambient pressure, as shown in Fig. 18. Furthermore, the variation of pressure wave behavior with ambient pressure presented in this section can be considered together with the electrical characteristics studied in the previous sections. Although the experiments were AQ:10 performed using two different high-voltage pulse generators, both generators produce a plasma discharge, whose energy deposition is similar [Fig. 17(b)]. Furthermore, the pressure

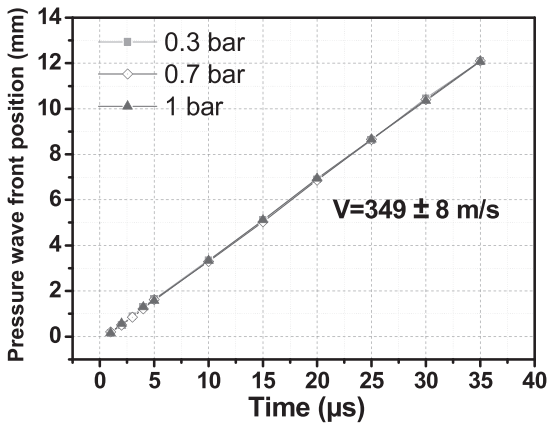

Fig. 19. Propagation speed of the pressure wave for different pressure levels.

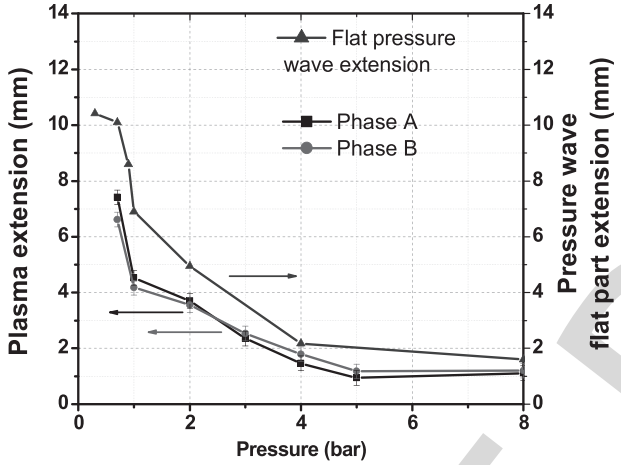

Fig. 20. Plasma layer extension and length of the planar part of the pressure wave at different pressure levels.

dependence is expected to be almost the same in both the cases, because the discharge energy follows the same empirical relationship with gas density, $U \sim N^{-0.5}$, whatever the generator used and the variation of the discharge extension length also follows the same relationship, $d \sim N^{-0.5}$.

The pressure wave is in fact composed of spherical and plane wave components, as observed in the previous experimental [1], [8], [12], [13] or numerical works [14], [18]. The spherical wave is seen to remain rather unchanged with pressure, but the plane wave diminishes in strength and length as the pressure increases from 300 to 1020 mbar. No change in the propagation speed of the pressure wave has been observed over the investigated range of pressure, all propagate at the speed of the sound (∼349 m/s) (Fig. 19). The spherical and plane waves result from rapid volumetric heating close to the electrode edge and along the surface, respectively. Thus, the energy dissipation must vary less with pressure close to the electrode edge than along the surface. Furthermore, as suggested in several papers, such as in [12] or [13], the planar part of the pressure wave results from the heat released during the propagation of filaments on the dielectric barrier surface. This is verified by plotting the plasma extension length together with the length of the planar part of the pressure wave for pressure from 300 mbar to 8 bar (Fig. 20). Both quantities follow the same behavior with close values. This confirms again the good correlation between the length of the planar part of the pressure wave and the extension of the plasma layer, confirming that the planar component of the induced pressure wave is due to the filaments that propagate along the dielectric surface [12].

IV. Conclusion

In this paper, we have investigated the electrical characteristics generated by NP-DBDs in the air, as a function of pressure (265–1020 mbar), temperature (from -50 °C to 20 °C), and altitude (0–10 km). The altitude conditions were reproduced using the appropriate pressure and temperature conditions. We found that the pressure has a much greater effect on plasma characteristics than the temperature. Temperature-specific effects are limited to an increase in the ignition delay time of the discharge with a decreasing temperature, but no significant influence on the discharge was observed. Since the pressure varies much more than the temperature with altitude (and because the change in pressure produces larger changes in gas density than the change in temperature), the changes in discharge characteristics with altitude closely track those of changes in pressure. One important result is that the deposited energy increases with altitude, suggesting that the NP-DBD can be operated at high altitude and probably be effective for flow control. In fact, most of the variations across all the cases can be explained by changes in the gas density rather than independent pressure or temperature effects, in particular, the deposited energy and the plasma extension scale with $N^{-0.5}$. This implies that test chambers where only the gas density can be varied are sufficient to simulate altitude conditions only as a first approximation. However, at low temperature as incurred at high altitude, the permittivity of the dielectric barrier is affected by the environmental conditions and the density matching is no more valid.

The pressure wave issuing from the fast heat release caused by the filaments of the nanosecond discharge has been characterized for low- and high-pressure conditions. In all the cases, a pressure wave propagating at the speed of sound is observed. The primary modifications of the pressure wave topology caused by the pressure relate to an increase in length of the planar part of the wave with increasing pressure. A good correlation is found between the increase of the planar part of the pressure wave and the length of the discharge.

Acknowledgment

The authors would like to thank A. Claverie for the help and fruitful discussions regarding the shadowgraphy method.

References

[1] D. V. Roupassov, A. A. Nikipelov, M. M. Nudnova, and A. Y. Starikovskii, "Flow separation control by plasma actuator with nanosecond pulsed-periodic discharge," *AIAA J.*, vol. 47, no. 1, pp. 168–185, 2009.

[2] J. Little, K. Takashima, M. Nishihara, I. Adamovich, and M. Samimy, "High lift airfoil leading edge separation control with nanosecond pulse DBD plasma actuators," in *Proc. 5th Flow Control Conf. AIAA*, 2010, paper 2010-4256.

[3] C. Rethmel, J. Little, K. Takashima, A. Sinha, I. Adamovich, and M. Samimy, "Flow separation control over an airfoil with nanosecond pulse driven DBD plasma actuators," in *Proc. 49th AIAA Aerosp. Sci. Meeting Including New Horizons Forum Aerosp. Expo.*, 2011, paper 2011-487.

[4] J. Little, K. Takashima, M. Nishihara, I. Adamovich, and M. Samimy, "Separation control with nanosecond-pulse-driven dielectric barrier discharge plasma actuators," *AIAA J.*, vol. 50, no. 2, pp. 350–365, 2012.

[5] I. Popov *et al.*, "Experimental study and numerical simulation of flow separation control with pulsed nanosecond discharge actuator," in *Proc. 51st AIAA Aerosp. Sci. Meeting Including New Horizons Forum Aerosp. Expo.*, 2013, paper 2013-572.

[6] A. Starikovskiy and R. Miles, "Dielectric barrier discharge control and flow acceleration enhancement by diode surface," in *Proc. 51st AIAA Aerosp. Sci. Meeting Including New Horizons Forum Aerosp. Expo.*, 2013, paper 2013-0754.

[7] I. V. Adamovich, J. Little, M. Nishihara, K. Takashima, and M. Samimy, "Nanosecond pulse surface discharges for high-speed flow control," in *Proc. 6th AIAA Flow Control Conf.*, 2012, paper 2012-3137.

[8] B. Arad, Y. Gazit, and A. Ludmirsky, "A sliding discharge device for producing cylindrical shock waves," *J. Phys. D, Appl. Phys.*, vol. 20, no. 3, p. 360, 1987.

[9] R. Ono and T. Oda, "Formation and structure of primary and secondary streamers in positive pulsed corona discharge—Effect of oxygen concentration and applied voltage," *J. Phys. D, Appl. Phys.*, vol. 36, no. 6, p. 1952, Jul. 2003.

[10] D. A. Xu, D. A. Lacoste, D. L. Rusterholtz, P. Q. Elias, G. D. Stancu, and C. O. Laux, "Experimental study of the hydrodynamic expansion following a nanosecond repetitively pulsed discharge in air," *Appl. Phys. Lett.*, vol. 99, no. 12, p. 121502, 2011.

[11] K. Takashima, Y. Zuzeek, W. R. Lempert, and I. V. Adamovich, "Characterization of a surface dielectric barrier discharge plasma sustained by repetitive nanosecond pulses," *Plasma Sour. Sci. Technol.*, vol. 20, no. 5, p. 055009, 2011.

[12] N. Benard, N. Zouzou, A. Claverie, J. Sotton, and E. Moreau, "Optical visualization and electrical characterization of fast-rising pulsed dielectric barrier discharge for airflow control applications," *J. Appl. Phys.*, vol. 111, no. 3, p. 033303, 2012.

[13] R. Dawson and J. Little, "Characterization of nanosecond pulse driven dielectric barrier discharge plasma actuators for aerodynamic flow control," *J. Appl. Phys.*, vol. 113, no. 10, p. 103302, 2013.

[14] X. Che, T. Shao, W. Nie, and P. Yan, "Numerical simulation on a nanosecond-pulse surface dielectric barrier discharge actuator in near space," *J. Phys. D, Appl. Phys.*, vol. 45, no. 14, p. 145201, Mar. 2012.

[15] A. Starikovskiy and S. Pancheshnyi, "Dielectric barrier discharge development at low and moderate pressure conditions," in *Proc. 51st AIAA Aerosp. Sci. Meeting Including New Horizons Forum Aerosp. Expo.*, 2013, paper 2013-0902.

[16] N. Benard and E. Moreau, "Effects of altitude on the electromechanical characteristics of a single dielectric barrier discharge plasma actuator," in *Proc. 41st Plasmadyn. Lasers Conf. AIAA*, 2010, paper 2010-4633.

[17] D. E. Ashpis and D. R. Thurman, "DBD plasma actuators for flow control in air vehicles and jet engines-simulation of flight conditions in test chambers by density matching," in *Proc. 42nd AIAA Plasmadyn. Lasers Conf.*, 2011, paper AIAA-2011-3730.

[18] T. Unfer and J.-P. Boeuf, "Modeling and comparison of sinusoidal and nanosecond pulsed surface dielectric barrier discharges for flow control," *Plasma Phys. Controlled Fusion*, vol. 52, no. 10, p. 124019, Nov. 2010.

Nicolas Benard received the Ph.D. degree in aerodynamic and turbulence from the Université de Poitiers, Poitiers, France, in 2005.

He was an Associate Professor with the Electrical Engineering Department, Université de Poitiers, in 2008. He is a Coordinator of the INOPLAS national research program and was the WP Leader of the MARS EU project. He has authored over 50 full papers in the last six years and participated in about 60 international conferences related to control of laminar and turbulent flows by plasma actuation. His main technical expertise is in development of innovative plasma actuators with interest for their use as flow control devices in open and closed-loop approaches.

Kossi Djidula Bayoda was born in Lomé, Togo, in 1989. He received the M.Sc. degree in energy management from the Université de Poitiers, Poitiers, France, in 2013, where he is currently pursuing the Ph.D. degree in electrical engineering with the Institut Pprime.

His current research interests include nonthermal plasma technology, electrostatic hazards, and active flow control.

Arthur Claude Aba'a Ndong was born in Libreville, Gabon, in 1983. He received the M.Sc. degree in industrial systems engineering and electrical engineering and the Ph.D. degree in electrical engineering from the Université de Poitiers, Poitiers, France, in 2011 and 2014, respectively.

He currently holds a post-doctoral position with the Institut Universitaire de Technologie d'Angoulême, Angoulême, France, where he is involved in particle precipitation and collection by plasma discharge. His current research interests include the applications of electrostatics, nonthermal plasma technology, air pollution control, and electrostatic hazards.

Eric Moreau received the Ph.D. degree in electrical engineering from the Université de Poitiers, Poitiers, France, in 1997.

He became an Assistant Professor with the Université de Poitiers in 1998, where he is currently a Full Professor of Electrical Engineering. He is mainly known for his works on plasma actuators for airflow control, but a part of his research is dedicated to corona-based thrusters and electrostatic precipitation of particles. He has been involved in several European projects, such as CAFEDA, AVERT, OPENAIR, PLASMAERO, MARS, and ORINOCO, and national projects, such as COS, INCA, SINAPS, and INOPLAS. He has authored or co-authored over 100 peer-reviewed articles in international journals and 150 papers in conference proceedings. His current research interests include electrohydrodynamics (EHD), especially the mechanical effects in atmospheric discharges (EHD force, ionic wind, and particle precipitation).

Prof. Moreau is a member of the Advisory Board of the LABEX INTERACTIFS National Grant.

AUTHOR QUERIES

AQ:1 = Please revise the phrase "In the final part" for clarity.
AQ:2 = Please supply index terms/keywords for your paper. To download the IEEE Taxonomy, go to http://www.ieee.org/documents/taxonomy_v101.pdf.
AQ:3 = Please confirm whether the edits made in the current affiliation are OK.
AQ:4 = Please confirm the postal code for "Université de Poitiers."
AQ:5 = Please provide the expansions for the acronyms "ICCD, PMMA, NS, and FID."
AQ:6 = Can the phrase "the authors" be changed to "us?" Please confirm.
AQ:7 = Please confirm whether the edited caption of Fig. 8 is appropriate.
AQ:8 = Please check whether the edits made in the sentence, "This corroborates with the study in [17] …" retain the intended meaning.
AQ:9 = The phrase "In this final part of the paper" has been changed to "In Section IV." Please confirm.
AQ:10 = Please indicate the section numbers for the phrase "the previous sections."
AQ:11 = Please provide the page range for refs. [1], [2], [5]–[7], and [15]–[17].
AQ:12 = Please confirm the retention of the text "His main technical expertise … closed-loop approaches." is OK.
AQ:13 = Current affiliation in biography of "Arthur Claude Aba'a Ndong" does not match First Footnote. Please check.
AQ:14 = Please confirm the retention of the text "He is mainly known for … precipitation of particles." is OK.
AQ:15 = Please confirm whether the edits made in the sentence "His current research interests … precipitation)." are OK.
AQ:16 = Please confirm whether the edits made in the sentence "Prof. Moreau is a member … National Grant." are OK.